Mbd3/NuRD controls lymphoid cell fate and inhibits tumorigenesis by repressing a B cell transcriptional program

Stephen J. Loughran,[1,2] Federico Comoglio,[1,2] Fiona K. Hamey,[1,2] Alice Giustacchini,[4] Youssef Errami,[1,2] Eleanor Earp,[1,2] Berthold Göttgens,[1,2] Sten Eirik W. Jacobsen,[4,5] Adam J. Mead,[4] Brian Hendrich,[2,3] and Anthony R. Green[1,2]

[1]Department of Haematology, Cambridge Institute for Medical Research, [2]Wellcome Trust/MRC Stem Cell Institute, and [3]Department of Biochemistry, University of Cambridge, Cambridge, England, UK
[4]MRC Weatherall Institute of Molecular Medicine, University of Oxford, Oxford, England, UK
[5]Wallenberg Institute for Regenerative Medicine, Department of Cell and Molecular Biology and Department of Medicine Huddinge, Karolinska Institutet and Center for Hematology and Regenerative Medicine, Karolinska University Hospital Huddinge, Stockholm, Sweden

The Journal of Experimental Medicine

Differentiation of lineage-committed cells from multipotent progenitors requires the establishment of accessible chromatin at lineage-specific transcriptional enhancers and promoters, which is mediated by pioneer transcription factors that recruit activating chromatin remodeling complexes. Here we show that the Mbd3/nucleosome remodeling and deacetylation (NuRD) chromatin remodeling complex opposes this transcriptional pioneering during B cell programming of multipotent lymphoid progenitors by restricting chromatin accessibility at B cell enhancers and promoters. Mbd3/NuRD-deficient lymphoid progenitors therefore prematurely activate a B cell transcriptional program and are biased toward overproduction of pro–B cells at the expense of T cell progenitors. The striking reduction in early thymic T cell progenitors results in compensatory hyperproliferation of immature thymocytes and development of T cell lymphoma. Our results reveal that Mbd3/NuRD can regulate multilineage differentiation by constraining the activation of dormant lineage-specific enhancers and promoters. In this way, Mbd3/NuRD protects the multipotency of lymphoid progenitors, preventing B cell–programming transcription factors from prematurely enacting lineage commitment. Mbd3/NuRD therefore controls the fate of lymphoid progenitors, ensuring appropriate production of lineage-committed progeny and suppressing tumor formation.

INTRODUCTION

In metazoans, mature cells develop from multipotent progenitor cells, a process that requires activation of cell type–specific gene expression programs alongside repression of programs associated with other cell lineages. Gene expression is linked to the state of the associated chromatin, including how accessible enhancers and promoters are to the binding of transcription factors and the general transcription machinery. Chromatin accessibility is regulated by multiprotein chromatin remodeling complexes (CRCs), which control nucleosome position. CRCs are essential for normal differentiation of progenitors during development, but the mechanisms by which specific CRCs regulate chromatin accessibility and lineage fate decisions in multipotent progenitors remain poorly understood (Ho and Crabtree, 2010; Chen and Dent, 2014).

The differentiation of mammalian B and T lymphocytes is a powerful model system to study the cellular and molecular events that control multilineage differentiation. B and T lymphocytes are derived from hematopoietic stem cells (HSCs) in the bone marrow that have the ability to self-renew and the potential to differentiate into all blood cell lineages. During lymphopoiesis, HSCs first differentiate into lymphoid-primed multipotent progenitors (LMPPs). LMPPs retain the ability to form myeloid and lymphoid cells but lack megakaryocyte and erythroid potential (Adolfsson et al., 2005). LMPPs subsequently differentiate into common lymphoid progenitors, which have minimal ability to differentiate into myeloid cells. The expression of the cell surface protein Ly6D has recently been used to separate the heterogeneous common lymphoid progenitor population into the $Ly6D^-$ all-lymphoid progenitor (ALP) subpopulation, which retains both B and T cell potential, and the $Ly6D^+$ B cell–biased lymphoid progenitor (BLP) subpopulation. BLPs are derived from ALPs and subsequently give rise to B lineage cells (Inlay et al., 2009).

Correspondence to Anthony R. Green: arg1000@cam.ac.uk

Abbreviations used: ALP, all-lymphoid progenitor; ATAC-seq, assay for transposase-accessible chromatin by sequencing; BAF, Brg1-associated factors; BLP, B cell–biased lymphoid progenitor; ChIP-seq, chromatin immunoprecipitation sequencing; CRC, chromatin remodeling complex; ES, embryonic stem; ETP, early thymic progenitor; HSC, hematopoietic stem cell; ISP, immature single-positive; LMPP, lymphoid-primed multipotent progenitor; NuRD, nucleosome remodeling and deacetylation; qPCR, quantitative PCR; qRT-PCR, quantitative RT-PCR; T-ALL, T cell acute lymphoblastic lymphoma.

The Rockefeller University Press
J. Exp. Med. 2017 Vol. 214 No. 10 3085–3104
https://doi.org/10.1084/jem.20161827

To produce T cells, ALPs that express the CC-chemokine receptors Ccr7 and Ccr9 and P-selectin glycoprotein ligand 1 (encoded by the gene *Selplg*) migrate to the thymus (Rossi et al., 2005; Inlay et al., 2009; Serwold et al., 2009; Schlenner et al., 2010; Zlotoff et al., 2010). Notch1 signaling is then activated in these progenitors by Delta-like protein 4(Dll4) on thymic stromal cells. This results in expression of transcription factors essential for T cell lineage commitment, including Hes1, and rapid loss of B cell lineage potential (Ceredig et al., 2007).

For the production of B cells, ALPs in the bone marrow first differentiate into BLPs, which requires expression of the E2A transcription factor (encoded by *Tcf3*; Inlay et al., 2009). E2A up-regulates the levels of the B cell–specifying pioneer transcription factor Ebf1. Ebf1, in association with the SWI/SNF CRC Brg1/BAF (Brg1-associated factors), induces the accessibility of chromatin at B cell lineage-specific enhancers and promoters (Bossen et al., 2015; Boller et al., 2016). Ebf1 also activates expression of Pax5, and these both then act with Foxo1 in a positive feedback loop (Mansson et al., 2012). Expression of these transcription factors results in commitment to the B cell lineage (Nutt et al., 1997; Ungerbäck et al., 2015).

Mbd3/nucleosome remodeling and deacetylation (Mbd3/NuRD) is a ubiquitously expressed CRC that contains the nucleosome-remodeling ATPase Chd4, a histone deacetylase (either Hdac1 or Hdac2), and several accessory proteins (Reynolds et al., 2013). Mbd3/NuRD has long been accepted as a transcriptional repressor (Ahringer, 2000; McDonel et al., 2009), but more recent data have shown that Mbd3/NuRD is prevalent at enhancers and promoters of active gene loci, and the presence of Mbd3/NuRD is as likely to be associated with active transcription as repressed transcription (Reynolds et al., 2013; Menafra and Stunnenberg, 2014; Miller et al., 2016). Mbd3 is a key structural element of Mbd3/NuRD, essential for stable assembly of the complex (Kaji et al., 2006). In mouse embryos lacking Mbd3, the inner cell mass of the blastocyst fails to differentiate into a mature epiblast (Kaji et al., 2007). In embryonic stem (ES) cells, Mbd3/NuRD at active enhancers and promoters limits expression of pluripotency-associated genes to enable successful lineage commitment and is present during the silencing and decommissioning of pluripotency gene enhancers during differentiation (Kaji et al., 2006; Reynolds et al., 2012a; Whyte et al., 2012; Miller et al., 2016). Because Mbd3-deficient ES cells do not undergo lineage-specific differentiation, the mechanisms by which Mbd3/NuRD-mediated chromatin remodeling may regulate lineage fate decisions are unclear.

Several Mbd3/NuRD subunit proteins regulate hematopoiesis. The Mbd3/NuRD component Mta3 represses plasma cell-specific transcription in B cell lines (Fujita et al., 2004). Loss of Chd4 in HSCs results in erythroid differentiation and exhaustion of the stem cell compartment (Yoshida et al., 2008). Chd4 is also required in the thymus for differentiation of β-selected thymocytes and regulation of CD4 expression (Williams et al., 2004; Naito et al., 2007). Deletion of Hdac1 and Hdac2 in differentiating thymocytes prevents differentiation beyond the $CD4^-$ $CD8^-$ stage (Dovey et al., 2013; Heideman et al., 2013). However, Chd4, Hdac1, and Hdac2 each have functions independent from their roles in Mbd3/NuRD, so the specific function of the Mbd3/NuRD complex in hematopoiesis has remained unknown (Williams et al., 2004; Yang and Seto, 2008).

To investigate how chromatin remodeling regulates multilineage differentiation, we generated mice with hematopoietic cells that lack Mbd3/NuRD. We demonstrate that Mbd3/NuRD constrains transcriptional pioneering during B cell specification and thus regulates the B versus T cell lineage fate of bipotent lymphoid progenitors and prevents the development of T cell lymphoma. Our results therefore reveal that Mbd3/NuRD chromatin remodeling can protect the multipotency of progenitors during differentiation by opposing the activation of lineage-specific transcriptional programs.

RESULTS

Loss of Mbd3 destabilizes the NuRD complex in hematopoietic cells

To determine the role of Mbd3/NuRD-mediated chromatin remodeling in hematopoiesis, $Mbd3^{Flox/Flox}$ mice (Aguilera et al., 2011) were crossed with *Vav-cre* mice (Stadtfeld and Graf, 2005), resulting in pan-hematopoietic deletion. The *Mbd3* locus in the resulting $Mbd3^{\Delta H/\Delta H}$ mice showed efficient Cre-mediated recombination throughout all hematopoietic organs (Fig. 1 A). *Mbd3* mRNA was undetectable in $Mbd3^{\Delta H/\Delta H}$ HSCs, and Mbd3 protein was absent in $Mbd3^{\Delta H/\Delta H}$ bone marrow, spleen, and thymus (Fig. 1, B and C).

Mbd3 is required to maintain the stability of the NuRD complex and the abundance of a subset of NuRD components in ES cells (Kaji et al., 2006). We found that Mbd3 was necessary for the maintenance of normal levels of Chd4 in spleen and thymus and Mta2 in bone marrow and thymus (Fig. 1 C). Mbd3 was also required to maintain the interaction between Chd4 and Hdac1 in the bone marrow (Fig. 1 D). These results demonstrate that $Mbd3^{\Delta H/\Delta H}$ mice lack Mbd3 expression in hematopoietic cells and that loss of Mbd3 prevents the formation of stable NuRD complexes in these cells.

$Mbd3^{\Delta H/\Delta H}$ mice develop T cell acute lymphoblastic lymphoma

$Mbd3^{\Delta H/\Delta H}$ mice were born at the expected Mendelian frequency, and the peripheral blood contained cells belonging to all hematopoietic lineages (Fig. S1 A). Numbers of peripheral blood B and T lymphocytes were reduced in 4-wk-old mice but were normal in older mice (Fig. S1 B). As $Mbd3^{\Delta H/\Delta H}$ mice aged, they invariably developed large thymic tumors (Fig. 1, E and F). In 29% of cases, enlargement of the spleen and peripheral lymph nodes was also detected. Histopathological analysis showed that the diseased thymi contained a population of lymphoblasts with homogeneous morphology, loss of medullary and cortical architecture, a high proportion of mitotic figures, and numerous tingible body macrophages

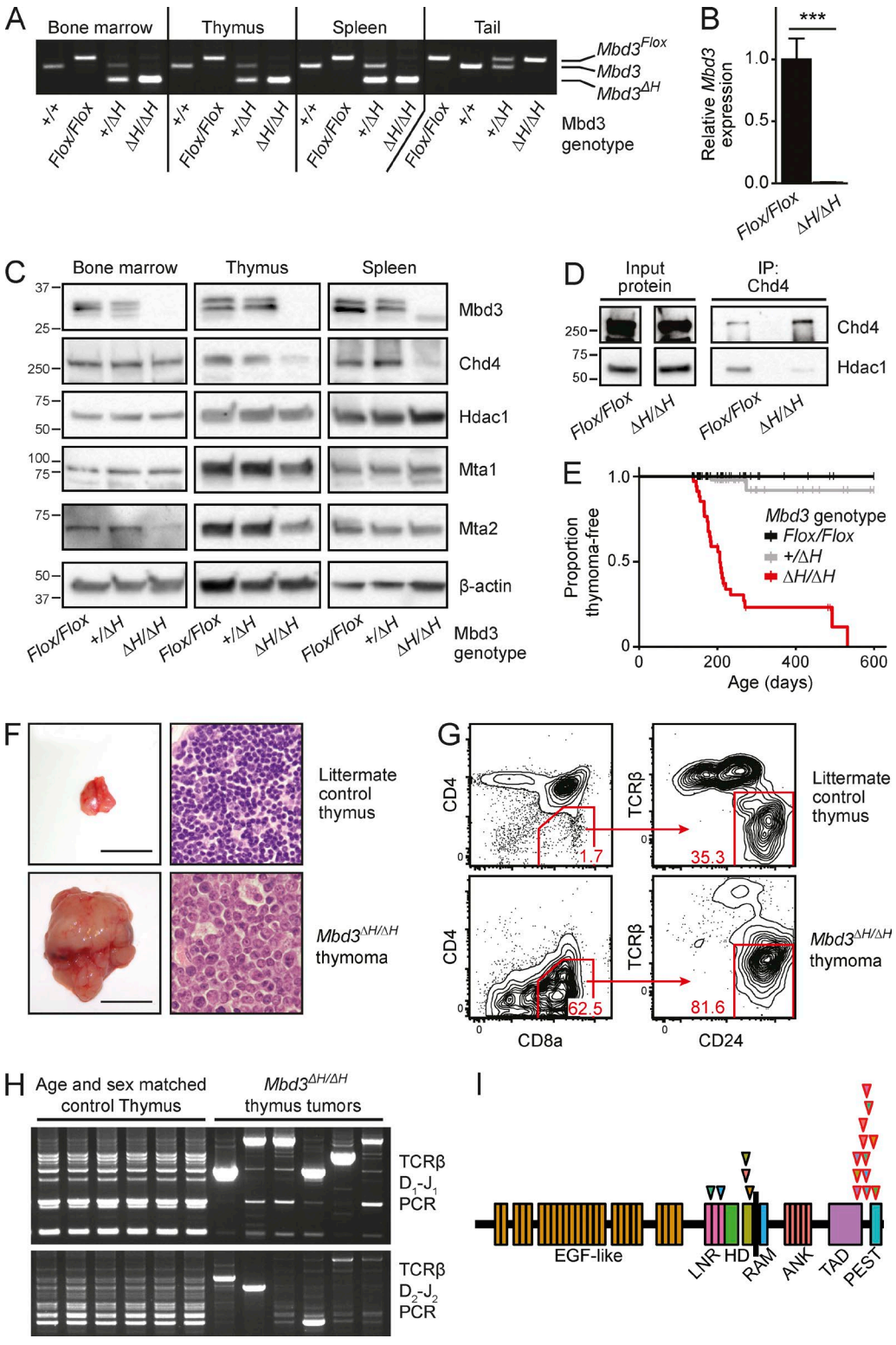

Figure 1. **Efficient deletion of Mbd3 in hematopoietic cells of *Mbd3*$^{\Delta H/\Delta H}$ mice destabilizes the NuRD complex and results in the development of T-ALL.** (A) PCR amplification of the Mbd3 locus from genomic DNA isolated from whole bone marrow, thymus, and spleen. Data shown are representative of at least three independent experiments using littermate mice. (B) Expression of *Mbd3* mRNA in CD150$^+$ CD48$^-$ EPCR$^+$ CD45$^+$ HSCs. Measured by quantitative RT-PCR, normalized to the expression of *Ubc*. Mean ± SE is shown, summarizing three independent experiments using littermate mice. ***, $P < 0.005$, Welch's *t* test. (C) Western blots of nuclear extracts, detecting NuRD complex proteins in whole bone marrow, spleen, and thymus. The antibodies used for

(Fig. 1 F). These features are characteristic of T cell acute lymphoblastic lymphoma (T-ALL).

FACS analysis of *Mbd3*$^{\Delta H/\Delta H}$ thymic tumors indicated that the majority of cells were CD8a^{+} CD4^{-} TCRβ^{-} CD24^{hi} (Fig. 1 G). This phenotype is identical to that of immature single-positive (ISP) T cell progenitors, which arise during the transition from CD4^{-} CD8^{-} double-negative to CD4^{+} CD8^{+} double-positive thymocytes during T cell differentiation. To confirm that the thymic masses were indeed clonal tumors and did not reflect hyperplasia of immature thymocytes, we analyzed Dβ$_1$-Jβ$_1$ and Dβ$_2$-Jβ$_2$ rearrangement at the TCRβ locus (Fig. 1 H). The majority of cells in the *Mbd3*$^{\Delta H/\Delta H}$ tumors had a single recombination event, indicating that they were clonally derived.

Activating mutations in *NOTCH1* are detected in >50% of human T-ALLs (Aster et al., 2011). Mutations in the coding sequence of *Notch1* were detected in 10 of 15 *Mbd3*$^{\Delta H/\Delta H}$ T-ALL tumors, affecting the heterodimerization domain or resulting in loss of the PEST domain (Fig. 1 I and Fig. S2 A). Such mutations are common in human T-ALL and result in hyperactivation of Notch signaling (Aster et al., 2011). We also detected genomic deletions in the 5′ region of *Notch1* in 6 *Mbd3*$^{\Delta H/\Delta H}$ T-ALLs (5 of which also had *Notch1* coding mutations; Fig. S2 B). These deletions cause alternative transcription that increases active intracellular Notch1 levels in murine T-ALL (Ashworth et al., 2010). Hyperactivation of Notch signaling in *Notch1* mutant *Mbd3*$^{\Delta H/\Delta H}$ lymphoma was confirmed by the up-regulation of Notch target genes *Hes1*, *Dtx1*, and *Myc* (Fig. S2 C).

Mbd3/NuRD is required to generate normal numbers of early T cell progenitors

Predisposition to T-ALL is often associated with defects in T cell differentiation (Yui and Rothenberg, 2014). Discrete stages of T cell maturation in the thymus can be identified by the expression of characteristic cell surface proteins (Fig. 2 A). At 8 wk of age, more than 2 mo before the earliest detection of thymic transformation, no significant differences in T cell differentiation were detected between *Mbd3*$^{Flox/Flox}$ and *Mbd3*$^{+/\Delta H}$ thymi, indicating that a single intact allele of Mbd3 is sufficient for normal T cell differentiation (Fig. 2, C and E–G). Thymi from *Mbd3*$^{\Delta H/\Delta H}$ mice exhibited a normal cell count (Fig. S1 C). However, FACS analysis revealed a marked reduction in the numbers of early T cell progenitors, including Flt3^{+} early thymic progenitors (ETPs), which are the most immature thymic cells, derived from the progenitors that migrate from the bone marrow to sustain thymopoiesis (Luc et al., 2012). The subsequent Flt3^{-} ETP, DN2, DN3, and DN4 thymic progenitors were also reduced (Fig. 2, B and C). Despite this severe deficit in the number of early T cell progenitors, *Mbd3*$^{\Delta H/\Delta H}$ thymi contained normal numbers of CD4^{+} CD8^{+} double-positive thymocytes that constitute the majority of the thymus (Fig. 2, D and E) as well as normal numbers of mature CD4^{+} CD8^{-} helper T cells (Fig. 2 D). Moreover, *Mbd3*$^{\Delta H/\Delta H}$ thymi contained significantly more CD4^{-} CD8^{+} cells as a consequence of drastically increased numbers of ISP thymocytes and CD4^{-} CD8^{+} TCRβ^{int} CD24^{hi} cells (Fig. 2, D, F, and G). These latter two populations are transitional stages between the CD4^{-} CD8^{-} double-negative thymocytes, which were drastically reduced, and CD4^{+} CD8^{+} double-positive thymocytes, which were present in normal numbers.

Our data indicate that Mbd3/NuRD is required to maintain the supply of normal numbers of bone marrow–derived T cell progenitors to the thymus. These residual early progenitors undergo compensatory hyperproliferation at the ISP stage, thus maintaining normal thymus cellularity. Consistent with this hypothesis, a significantly larger proportion of *Mbd3*$^{\Delta H/\Delta H}$ ISP thymocytes were actively cycling (Fig. 2, H and I). Analysis of TCR gene rearrangement in older mice before onset of T-ALL confirmed that the small number of *Mbd3*$^{\Delta H/\Delta H}$ early T cell progenitors in the thymus retain sufficient function to maintain polyclonal T lymphopoiesis for long periods of time (Fig. 2 J).

Mbd3/NuRD prevents precocious B cell differentiation of B/T-bipotent lymphoid progenitors

The number of lymphoid progenitors in the bone marrow capable of seeding the thymus was analyzed by flow cytometry (Fig. 3 A). Deletion of both alleles of *Mbd3* had no detectable effect on bone marrow cellularity (Fig. S1 D), number of HSCs, or number of LMPPs (Fig. 3 B). However, compared with littermate controls, *Mbd3*$^{\Delta H/\Delta H}$ bone marrow

protein detection are shown to the right of each blot, and protein size markers (kD) are shown on the left. Data shown are representative of at least three independent experiments using littermate mice. (D) Coimmunoprecipitation of Chd4 and Hdac1 from whole–bone marrow nuclear extracts. Antibodies used for immunoblotting are shown to the right of each blot, and protein size markers (kD) are shown on the left. All the images in this panel are from the same blot, which was first immunoblotted for Hdac1, then stripped and reprobed for Chd4. Several irrelevant lanes between those shown have been omitted. Data shown are representative of two independent experiments using littermate mice. (E) Kaplan-Meier survival curve, showing the age at which mice became moribund because of thymoma. (F) Enlarged thymus representative of *Mbd3*$^{\Delta H/\Delta H}$ tumors, compared with thymus from sex-matched littermate controls (left; bar, 1 cm). Representative hematoxylin and eosin–stained sections were photographed at 400× magnification (right). Data are representative of four independent experiments using littermate mice. (G) FACS analysis of representative *Mbd3*$^{\Delta H/\Delta H}$ thymus tumor, compared with sex-matched littermate control. The percentage of cells in each plot that lie within the each gate is shown. Data are representative of three independent experiments analyzing six tumor samples and six age- and sex-matched mice from the same mouse colony. (H) Analysis of Dβ$_1$-Jβ$_1$ and Dβ$_2$-Jβ$_2$ rearrangements at the *Tcrb* locus by PCR of genomic DNA from the indicated tissues. Data shown summarize six independent DNA extractions using age- and sex-matched mice from the same mouse colony. (I) Schematic diagram of the Notch1 protein, showing the location of mutations detected in *Mbd3*$^{\Delta H/\Delta H}$ T-ALL. The color inside each arrowhead represents a single T-ALL. Arrowheads with red outlines indicate frameshift and nonsense mutations that disrupt the C terminus of the protein.

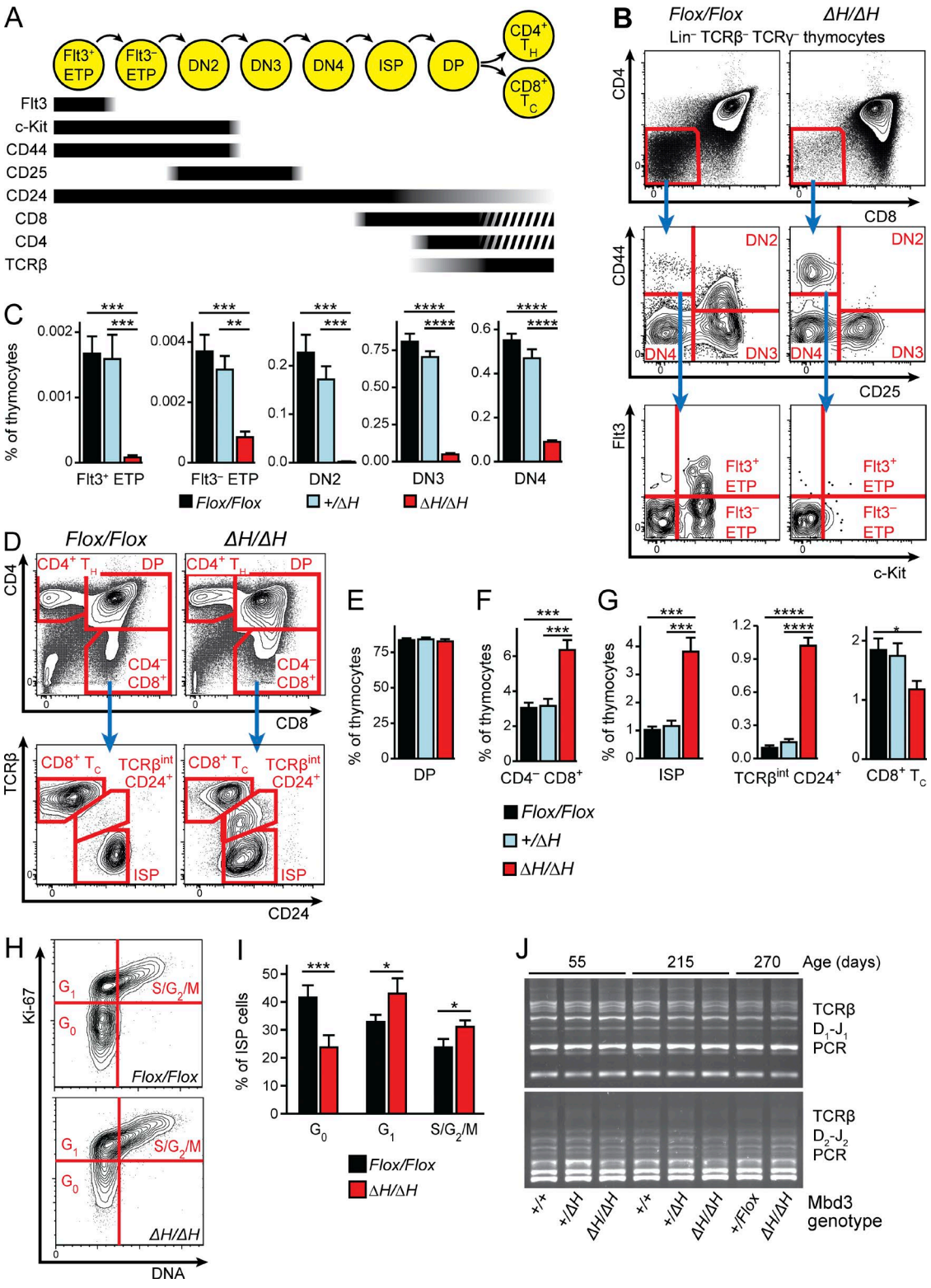

Figure 2. **Mbd3/NuRD-deficient thymus contains very few early T cell progenitors, but thymocyte numbers are maintained by an expanded population of hyperproliferating immature single-positive thymocytes.** (A) Schematic diagram showing cell surface antigen expression during key stages of thymocyte differentiation. (B) Representative FACS plots of $CD4^-$ $CD8^-$ double-negative cell subpopulations in Lin^- $TCR\beta^-$ $TCR\gamma\delta^-$ thymocytes. (C) The percentage of thymocytes in each of the $CD4^-$ $CD8^-$ double-negative subpopulations (mean ± SEM, $n = 6$). (D) Representative FACS plots showing CD4 and CD8 expression in thymocytes, as well as TCRβ and CD24 expression in $CD4^-$ $CD8^+$ thymocytes. (E) The percentage of thymocytes in the $CD4^+$ $CD8^+$

contained significantly fewer ALPs and BLPs (Fig. 3, B and C) and markedly increased numbers of B220$^+$ c-Kit$^+$ B cell precursors belonging to Hardy fractions A, B, and C (Fig. 3, D and E). Moreover, in *Mbd3*$^{\Delta H/\Delta H}$ mice, a larger proportion of fraction B and C cells expressed c-Kit (Fig. 3 F), including fraction B and C cells with high levels of c-Kit that were not present in control bone marrow (Fig. S3). This indicates that genes associated with B-lineage commitment, including CD19 and BP-1, are expressed before the repression of genes, such as *Kit*, that are normally down-regulated during B-lineage differentiation.

Collectively, these findings were compatible with loss of Mbd3/NuRD causing early bipotent lymphoid progenitors to undergo precocious B cell differentiation, resulting in fewer cells with an ALP and BLP phenotype. To test this hypothesis, LMPPs and ALPs were isolated by flow cytometry and subjected to B cell and T cell differentiation-inducing conditions in vitro. No significant differences were found in the potential of single *Mbd3*$^{Flox/Flox}$ and *Mbd3*$^{\Delta H/\Delta H}$ LMPPs or ALPs to generate B or T cells when placed in appropriate in vitro conditions (Fig. 4, A and B). However, *Mbd3*$^{\Delta H/\Delta H}$ LMPPs and ALPs consistently differentiated into B220$^+$ CD19$^+$ B cells more rapidly than controls (Fig. 4, C–E). This effect was most striking in *Mbd3*$^{\Delta H/\Delta H}$ ALPs, in which a substantial proportion of cells were B220$^+$ CD19$^+$ within 3 d of culture, whereas even small numbers of B220$^+$ CD19$^+$ cells were not present in control ALP cultures until 6 d. During B cell differentiation, prepro–B cells first up-regulate B220, then pro–B cells express both B220 and CD19 (Rumfelt et al., 2006). *Mbd3*$^{\Delta H/\Delta H}$ ALP cultures contained a lower proportion of B220$^+$ CD19$^-$ cells during differentiation, consistent with the concept that once B cell differentiation begins in these cells, it proceeds abnormally rapidly (Fig. 4 F). These results demonstrate that *Mbd3*-null multipotent lymphoid progenitors are poised to undergo premature B cell differentiation.

Mbd3$^{\Delta H/\Delta H}$ LMPPs and ALPs differentiated into T cell progenitors in vitro at a normal rate, indicating that the rapid differentiation phenomenon is limited to the B cell lineage (Fig. 4 G). *Mbd3*$^{\Delta H/\Delta H}$ LMPPs and ALPs also express normal levels of the Ccr7 and Ccr9 chemokine receptors that mediate migration from the bone marrow to the thymus (Fig. 4 H). Together these data suggest that Mbd3/NuRD-deficient lymphoid progenitors retain the ability to migrate to the thymus and undergo T cell differentiation but are predisposed to differentiate rapidly down the B cell lineage.

Mbd3/NuRD restrains the B cell commitment-associated transcriptional program

To determine whether the propensity of *Mbd3*$^{\Delta H/\Delta H}$ ALPs to commit prematurely to the B cell lineage was associated with dysregulation of lineage-affiliated genes, we measured expression levels of 48 genes (Table S1), including B cell, T cell, and myeloid lineage-associated genes, transcriptional regulators, and NuRD components, in single HSCs, LMPPs, ALPs, and BLPs sorted from *Mbd3*$^{\Delta H/\Delta H}$ and control mice. A subset of *Mbd3*$^{\Delta H/\Delta H}$ ALPs displayed an abnormal gene expression pattern closely resembling BLPs (Fig. 5 A). Moreover, pseudotemporal ordering of cells along a differentiation trajectory based on their gene expression profiles revealed that *Mbd3*-null LMPPs and ALPs possessed transcriptional states associated with later stages of differentiation (Fig. 5 B; and Fig. S4, A and B). Analysis of the genes that correlated with differentiation showed that *Ebf1*, *Cd79a*, *Pax5*, and *Igll1* were expressed in a higher proportion of *Mbd3*$^{\Delta H/\Delta H}$ ALPs compared with control ALPs (Fig. 5 C; and Fig. S4, C and D). Ebf1 is a pioneer transcription factor that instructs the B cell programming of lymphoid progenitors (Boller et al., 2016). *Cd79a*, *Pax5*, and *Igll1* are B cell lineage-specific Ebf1 targets that should be silent in ALPs (Maier et al., 2004; Zandi et al., 2008; Decker et al., 2009). Although the levels of Ebf1 expression were not significantly higher in individual *Mbd3*-null ALPs (Fig. S4 E), single *Mbd3*$^{\Delta H/\Delta H}$ ALPs frequently coexpressed *Ebf1* and its target genes (Fig. 5 D), indicating that Mbd3/NuRD chromatin remodeling limits the ability of Ebf1 to activate transcription in multipotent lymphoid progenitor cells.

To further investigate the transcriptional consequences of Mbd3 loss, we performed global transcriptional profiling of HSCs, LMPPs, ALPs, and BLPs by RNA sequencing (RNA-seq). Differences in gene expression between cell types were much larger than differences caused by Mbd3 deletion, indicating that the overall transcriptional identity of these cells was not grossly aberrant in the absence of Mbd3/NuRD (Fig. 6 A; and Tables S5, S6, S7, and S8). However, the set of genes up-regulated during the differentiation of control ALPs to control BLPs (Fig. 6 B) was expressed at significantly higher levels in *Mbd3*$^{\Delta H/\Delta H}$ ALPs compared with control ALPs (Fig. 6 C). The leading-edge subset of these BLP-specific genes that are enriched in *Mbd3*$^{\Delta H/\Delta H}$ ALPs includes B cell–specific genes such as transcription factors (*Ebf1*, *Pou2af1*) and components of the preB cell receptor

double-positive (DP) thymocyte population. Data are shown as the mean percentage of total thymocytes ± SEM; $n = 6$. (F) The percentage of thymocytes in the CD4$^-$ CD8$^+$ population. Data are shown as the mean percentage of total thymocytes ± SEM; $n = 6$. (G) The percentage of thymocytes in the ISP (CD4$^-$ CD8$^+$ TCR$^-$ CD24$^+$), CD8+ T$_c$ (CD4$^-$ CD8$^+$ TCR$^+$ CD24$^-$), and CD4$^-$ CD8$^+$ TCR^{int} CD24$^+$ populations of CD4$^-$ CD8$^+$ single-positive thymocytes. Data are shown as the mean percentage of total thymocytes ± SEM; $n = 5$. Data shown in B–G represent five independent experiments using littermate control mice. (H) Representative FACS plots showing Ki-67 expression and DNA content in ISP thymocytes. Cells in the G_0, G_1, and $S/G_2/M$ phases are indicated. (I) The percentage of ISP cells in the G_0, G_1, and $S/G_2/M$ phases of the cell cycle (mean ± SEM; $n = 4$). Data shown in H and I represent two independent experiments using littermate control mice. (J) Analysis of Dβ_1-Jβ_1 and Dβ_2-Jβ_2 rearrangements at the *Tcrb* locus by PCR of genomic DNA from thymus. Data from three independent DNA isolations are shown, and this is one representative of two independent experiments. *, $P < 0.05$; **, $P < 0.01$; ***, $P < 0.005$; and ****, $P < 0.001$ (Welch's *t* test with Benjamini-Hochberg p-value adjustment to correct for multiple testing).

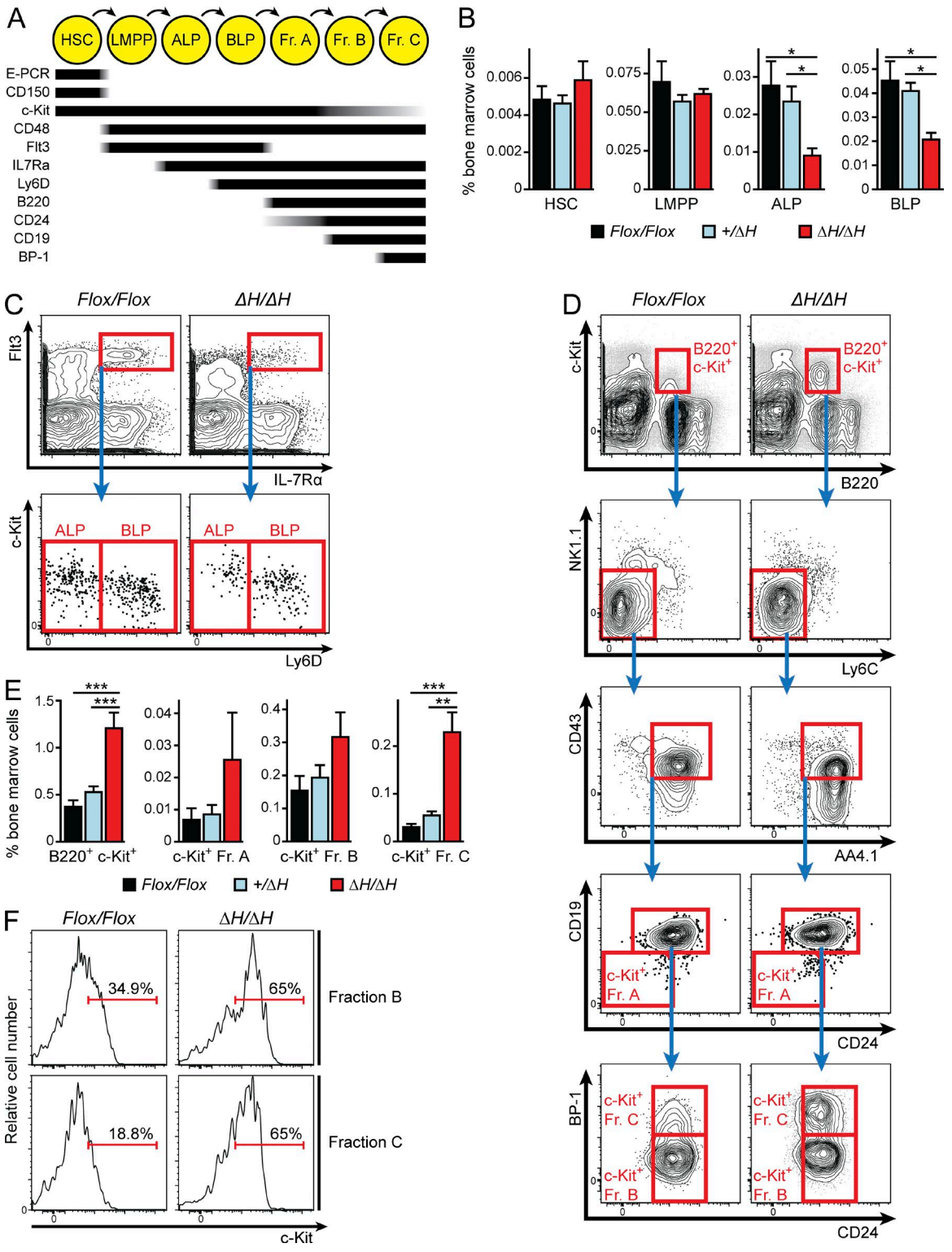

Figure 3. **Mbd3/NuRD maintains normal numbers of B/T-bipotent lymphoid progenitor cells and restricts the number of c-Kit⁺ pro–B cells.** (A) Schematic diagram showing cell surface antigen expression during key stages of early B cell differentiation. (B) The percentage of nucleated bone marrow cells belonging to the following populations: hematopoietic stem cell (HSC; CD150⁺ CD48⁻ CD45⁺ EPCR⁺), lymphoid-primed multipotent progenitor (LMPP; Lin⁻ B220⁻ c-Kit⁺ Sca-1⁺ Flt3^{hi} IL7Rα⁻), all-lymphoid progenitor (ALP; Lin⁻ B220⁻ Flt3^{hi} IL7Rα⁺ Ly6D⁻), and B-biased lymphoid progenitor (BLP; Lin⁻ B220⁻ Flt3^{hi} IL7Rα⁺ Ly6D⁺). Mean ± SEM is shown; $n = 6$ for HSC, $n = 5$ for LMPP, ALP, and BLP). (C) Representative FACS plots of the ALP and BLP populations within Lin⁻ B220⁻ bone marrow cells. (D) Representative FACS plots showing Hardy B cell progenitor fraction A (Fr. A; B220⁺ NK1.1⁻ Ly6C⁻ CD93⁺ CD43⁺

(*Cd79a*, *VpreB1*, *VpreB2* and *Igll1*; Fig. 6 D). Notably, the mRNA levels of *Ly6d* are 2.6-fold higher in $Mbd3^{\Delta H/\Delta H}$ ALPs (Fig. 6 D). These results indicate that $Mbd3^{\Delta H/\Delta H}$ ALPs have prematurely up-regulated the B cell transcriptional program and are poised to rapidly differentiate into $Ly6D^+$ BLPs.

Furthermore, the expression of the set of 31 genes down-regulated during the differentiation of control ALPs to BLPs (Fig. 6 B) is significantly higher in $Mbd3^{\Delta H/\Delta H}$ BLPs than control BLPs (Fig. 6 E). These data indicate that in the absence of Mbd3/NuRD, differentiation into BLPs occurs despite incomplete silencing of the ALP transcriptional program.

To confirm our results at the single-cell level, RNA-seq was performed on single LMPPs, ALPs, and BLPs obtained from normal and $Mbd3^{\Delta H/\Delta H}$ mice. We identified 289 genes that were differentially expressed between normal LMPPs and BLPs (Table S9). Dimensionality reduction analyses of this gene set allowed comparison of the expression patterns of lymphoid differentiation-associated genes in individual $Mbd3^{Flox/Flox}$ and $Mbd3^{\Delta H/\Delta H}$ cells (Fig. 6 F). The results identified a subset of $Mbd3^{\Delta H/\Delta H}$ ALPs with an aberrant gene expression pattern more similar to that of BLPs. Further analysis of single-cell RNA-seq data identified 90 genes differentially expressed in $Mbd3^{\Delta H/\Delta H}$ ALPs compared with $Mbd3^{Flox/Flox}$ ALPs (false discovery rate < 0.05), including up-regulation of *Ebf1* and its targets *Cd79a* and *Igll1* and down-regulation of the T cell receptor signaling kinase *Lck* (Table S10). This is consistent with the higher proportion of individual $Mbd3^{\Delta H/\Delta H}$ ALPs expressing *Ebf1* and its target genes detected by single-cell quantitative PCR (qPCR; Fig. 5, C and D).

Three independent sets of gene expression data (single-cell qPCR, RNA-seq on sorted populations, and single cell RNA-seq) therefore demonstrate that Mbd3-null ALPs prematurely activate an early B cell transcriptional program. The premature activation of B cell–specific genes in Mbd3-deficient progenitors is consistent with their propensity to rapidly differentiate into B cells.

Mbd3/NuRD restricts chromatin accessibility during B cell specification

Mbd3/NuRD regulates gene expression by binding to enhancer and promoter chromatin regions and remodeling them to make them less accessible to the transcriptional machinery (Yildirim et al., 2011). Chromatin accessibility changes significantly during B cell specification as a de novo enhancer and promoter repertoire is established (Bossen et al., 2015; Boller et al., 2016). Chromatin at these regions is inaccessible in ALPs and is made more accessible by transcriptional pioneering during differentiation into pro–B cells (Bossen et al., 2015). We used the assay for transposase-accessible chromatin by sequencing (ATAC-seq; Buenrostro et al., 2013) to measure chromatin accessibility in lymphoid progenitors from $Mbd3^{\Delta H/\Delta H}$ and control mice. Mbd3-null ALPs, BLPs, and pro–B cells all exhibited more accessible chromatin regions compared with $Mbd3^{Flox/Flox}$ controls (Fig. 7 A and Table S11). The $Mbd3^{\Delta H/\Delta H}$-specific accessible regions were most frequently associated with promoters, although an increased proportion of intergenic accessible regions associated with Mbd3 deletion was observed in pro–B cells (Fig. 7 B). The majority (70.6%) of $Mbd3^{\Delta H/\Delta H}$-specific accessible regions in ALPs were also accessible in $Mbd3^{Flox/Flox}$ pro–B cells, indicating that Mbd3 deletion causes premature accessibility of B cell–associated regulatory regions of chromatin during lymphoid differentiation (Fig. 7 C). Consistent with this, Gene Ontology analysis revealed that the $Mbd3^{\Delta H/\Delta H}$-specific accessible regions in BLPs and pro–B cells were associated with genes involved in B cell receptor signaling and the immune system (Fig. 7 D).

We further analyzed chromatin accessibility at the repertoire of enhancers and promoters active in pro–B cells, which has previously been determined by p300 chromatin immunoprecipitation sequencing (ChIP-seq; Visel et al., 2009; Lin et al., 2012). In control cells, the majority of pro–B cell enhancer and promoter regions were inaccessible in ALPs and BLPs and became accessible at the pro–B cell stage (Fig. 8, A and B). Loss of Mbd3/NuRD had no detectable effect on the accessibility of most of these regions in ALPs (probably because only a small subset of these regions are accessible at this stage) but resulted in a dramatic increase of accessibility in BLPs and pro–B cells (Fig. 8, A and B). Accessibility of pro-B enhancer regions and transcriptional start sites was unaltered in thymic T cell progenitors from $Mbd3^{\Delta H/\Delta H}$ mice, indicating that Mbd3/NuRD is specifically required in lymphopoiesis to regulate chromatin accessibility in the B cell lineage (Fig. S5). Analysis of ChIP-seq data for Chd4 in pro–B cells (Schwickert et al., 2014) at the same pro–B cell regions shown in Fig. 8 A indicated that most pro–B cell enhancer regions are bound by this factor, indicating they are directly bound by Mbd3/NuRD (Fig. 8 C).

The Brg1/BAF CRC is recruited to chromatin by B cell programming transcription factors including Ebf1, where it plays a key role in transcriptional pioneering during B cell differentiation, promoting nucleosome depletion and initiating chromatin accessibility (Gao et al., 2009; Bossen et al., 2015; Boller et al., 2016). By analyzing published ATAC-seq profiles (Bossen et al., 2015) from Brg1-null ALPs, BLPs, and

$CD24^{lo}$ $CD19^-$ c-Kit^+), fraction B ($B220^+$ $NK1.1^-$ $Ly6C^-$ $CD93^+$ $CD43^+$ $CD24^+$ $CD19^+$ $BP\text{-}1^-$), and fraction C ($B220^+$ $NK1.1^-$ $Ly6C^-$ $CD93^+$ $CD43^+$ $CD24^+$ $CD19^+$ $BP\text{-}1^+$) populations of c-Kit^+ bone marrow cells. (E) The percentage of nucleated bone marrow cells in the $B220^+$ c-Kit^+ population and in Hardy fraction A, c-Kit^+ fraction B, and c-Kit^+ fraction C (mean ± SEM; $n = 6$). (F) Representative FACS plots showing c-Kit expression in fraction B and fraction C cells. The percentage of cells inside the indicated gates is shown. *, $P < 0.05$; **, $P < 0.01$; and ***, $P < 0.005$ (Welch's *t* test with Benjamini-Hochberg p-value adjustment to correct for multiple testing). All data shown are from five independent experiments.

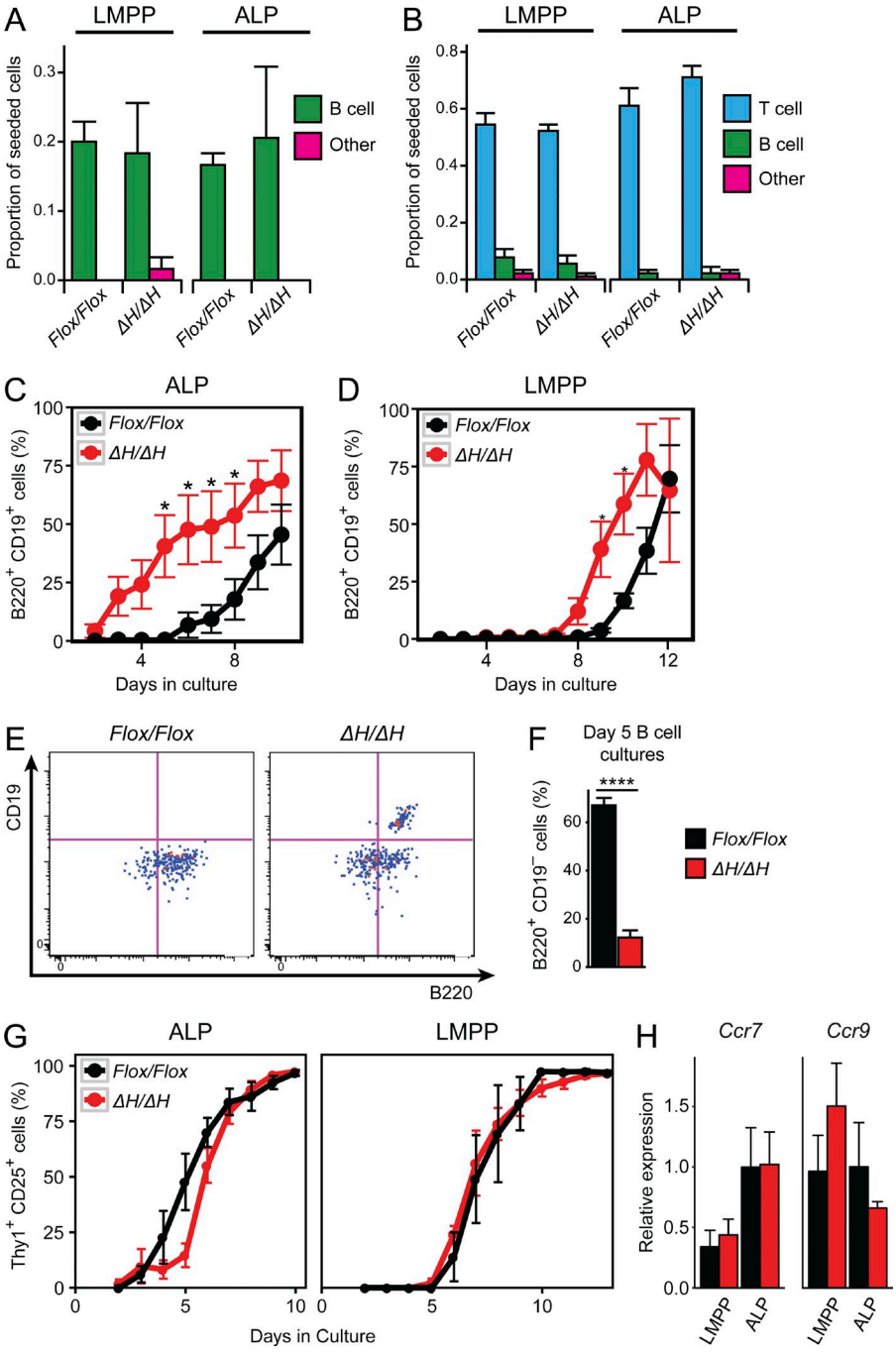

Figure 4. **Mbd3 prevents premature B lineage commitment of lymphoid progenitors.** (A) The proportion of single lymphoid progenitor cells with B cell potential when seeded in OP9 B differentiation co-culture conditions. The phenotype of the seeded cell is shown above each graph. The color of the bars indicates the phenotype of the single cell–derived colonies. Mean ± SEM of the proportion of single cells that formed colonies is shown; $n = 3$ independent experiments, each with 30 single cells seeded. (B) The proportion of single lymphoid progenitor cells with T cell potential when seeded in OP9-DL1 T differentiation co-culture conditions. The phenotype of the seeded cell is shown above each graph. The color of the bars indicates the phenotype of the single cell–derived colonies. Mean ± SEM of the proportion of single cells that formed colonies is shown; $n = 3$ independent experiments, each with 20 single cells seeded. (C) The percentage of $B220^+$ $CD19^+$ B cells in OP9 B differentiation co-cultures seeded by 50 ALPs, measured daily from day 2. Data are shown as mean ± SEM of the percentage of $B220^+$ $CD19^+$ B cells in each culture; $n = 9$ (three independent experiments, each with three biologically independent cultures). *, $P < 0.05$, Welch's t test, with Benjamini-Hochberg p-value adjustment to correct for multiple testing. (D) The percentage of $B220^+$ $CD19^+$ B cells in OP9 B differentiation co-cultures seeded by 50 LMPPs, measured daily from day 2. Data are shown as mean ± SEM of the percentage of $B220^+$ $CD19^+$ B cells in each culture; $n = 9$ (three independent experiments, each with three biologically independent cultures). *, $P < 0.05$, Welch's t test, with Benjamini-Hochberg p-value adjustment to correct for multiple testing. (E) Representative FACS plots of OP9 B differentiation cultures 4 d after seeding with 50 ALP cells. The gating of $B220^+$ $CD19^+$ B cells is shown. (F) The percentage of $B220^+$ $CD19^-$ cells in OP9 B differentiation co-cultures seeded with 50 ALPs or 50 LMPPs after 5 d in culture. Data are shown as mean ± SEM of the percentage of $B220^+$ $CD19^+$ B cells in each culture; $n = 9$ (three independent experiments, each with three biologically independent cultures). ****, $P < 0.001$, Welch's t test, with Benjamini-Hochberg p-value adjustment to correct for multiple testing. (G) The percentage of $Thy1^+$ $CD25^+$ T cell progenitors in OP9-DL1 T differentiation co-cultures seeded by 50 ALPs or 50 LMPPs, measured daily from day 2. Data are shown as mean ± SEM of the percentage of $Thy1^+$ $CD25^+$ cells in each culture; $n = 3$ biologically independent cultures. The data shown here are representative of two independent experiments. (H) Expression of *Ccr7* and *Ccr9* mRNA in $Mbd3^{Flox/Flox}$ (black) and $Mbd3^{\Delta H/\Delta H}$ (red) LMPPs and ALPs. Measured by quantitative RT-PCR, normalized to the expression of *Ubc*. Mean ± SE normalized to the level of expression in ALPs is shown; $n = 5$. Data are taken from five independent experiments.

pro–B cells at the same set of pro–B cell active enhancers and promoters shown in Fig. 8 A, we found that accessibility of these sites was lower in Brg1-null pro–B cells (Fig. 8 D). Together, these data indicate that Mbd3/NuRD binds to B cell–specific enhancers and promoters and provides repressive chromatin remodeling activity during the B cell specification of lymphoid progenitor cells, which opposes the activating activity of the Brg1/BAF complex.

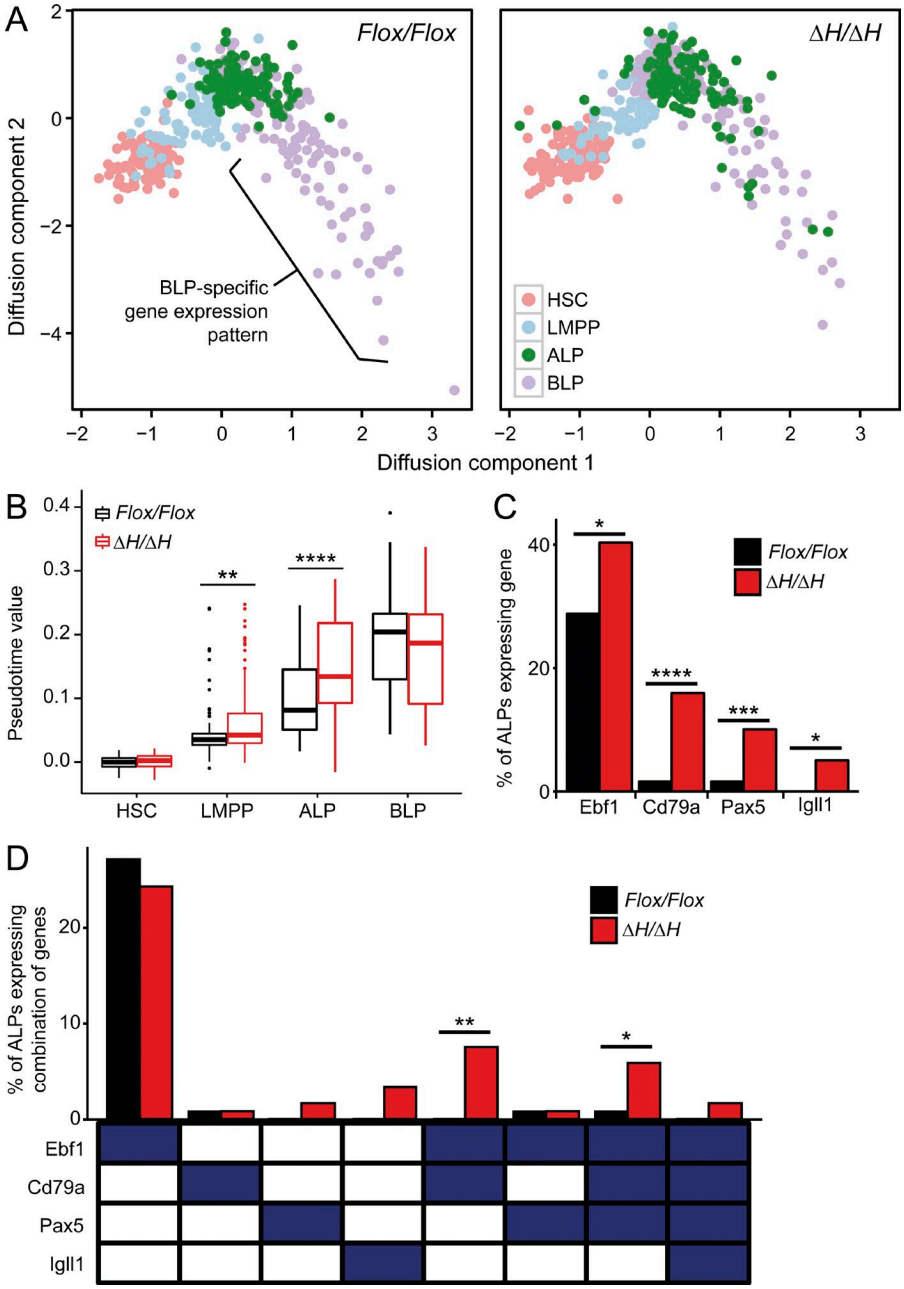

Figure 5. **Mbd3/NuRD prevents the premature expression of B cell lineage-specific Ebf1 target genes in single lymphoid progenitors.** (A) Diffusion map dimensionality reduction analysis of gene expression patterns in single HSCs, LMPPs, ALPs, and BLPs, measured by quantitative RT-PCR. Mapping was performed on *Mbd3*$^{Flox/Flox}$ and *Mbd3*$^{\Delta H/\Delta H}$ cells together, but cells of each genotype are depicted in separate plots. The region of the plot that contains cells with a gene expression pattern specific to control BLPs is indicated. (B) Pseudotime trajectory values of single HSCs, LMPPs, ALPs, and BLPs. Higher values indicate single cells with gene expression patterns associated with later stages of differentiation. Boxes indicate the interquartile range (IQR) of the pseudotime trajectory values in each population, the horizontal line indicates the median, and the vertical lines show the range of values. Outlier values more than 1.5 times the IQR outside the IQR are indicated by dots. **, $P < 0.01$; and ****, $P < 0.001$ (Wilcoxon rank sum test). (C) The percentage of single ALPs in which *Ebf1*, *Cd79a*, *Pax5*, and *Igll1* gene expression was detected. *, $P < 0.05$; ***, $P < 0.005$; and ****, $P < 0.001$ (Fisher's exact test). (D) The percentage of single ALPs in which combinations of *Ebf1*, *Cd79a*, *Pax5*, and *Igll1* gene expression were coexpressed. Blue boxes indicate that gene expression was detected. *, $P < 0.05$; and **, $P < 0.01$ (Fisher's exact test). All data in this figure are from single cells sorted from littermate mice in three independent experiments.

DISCUSSION

Lineage commitment of multipotent progenitors requires reorganization of chromatin accessibility to activate a lineage-specific transcriptional program while repressing genes associated with other cell fates (Mercer et al., 2011; Whyte et al., 2012; Lara-Astiaso et al., 2014). Here we demonstrate that Mbd3/NuRD constrains B cell specification by limiting chromatin accessibility and repressing a B cell transcriptional program. In this way, Mbd3/NuRD prevents lymphoid progenitors from precociously undergoing lineage commitment and ensures that appropriate numbers of progeny belonging to the B and T cell lineages are produced.

T cell progenitor deficiency in the Mbd3/NuRD-deficient thymus

Mbd3-null LMPPs and ALPs are able to differentiate into T cell progenitors in vitro at normal frequency and rate and express the chemokine receptors required for thymic migration. However, they are predisposed to rapidly differentiate into B cell lineage-committed progenitors. Our data therefore indicate that Mbd3/NuRD-deficient lymphoid progenitors retain the ability to seed the thymus with early T cell progenitors, but their propensity to prematurely commit to the B cell lineage gives them little opportunity to do so. As a result, few early T cell progenitors reach the *Mbd3*-null thy-

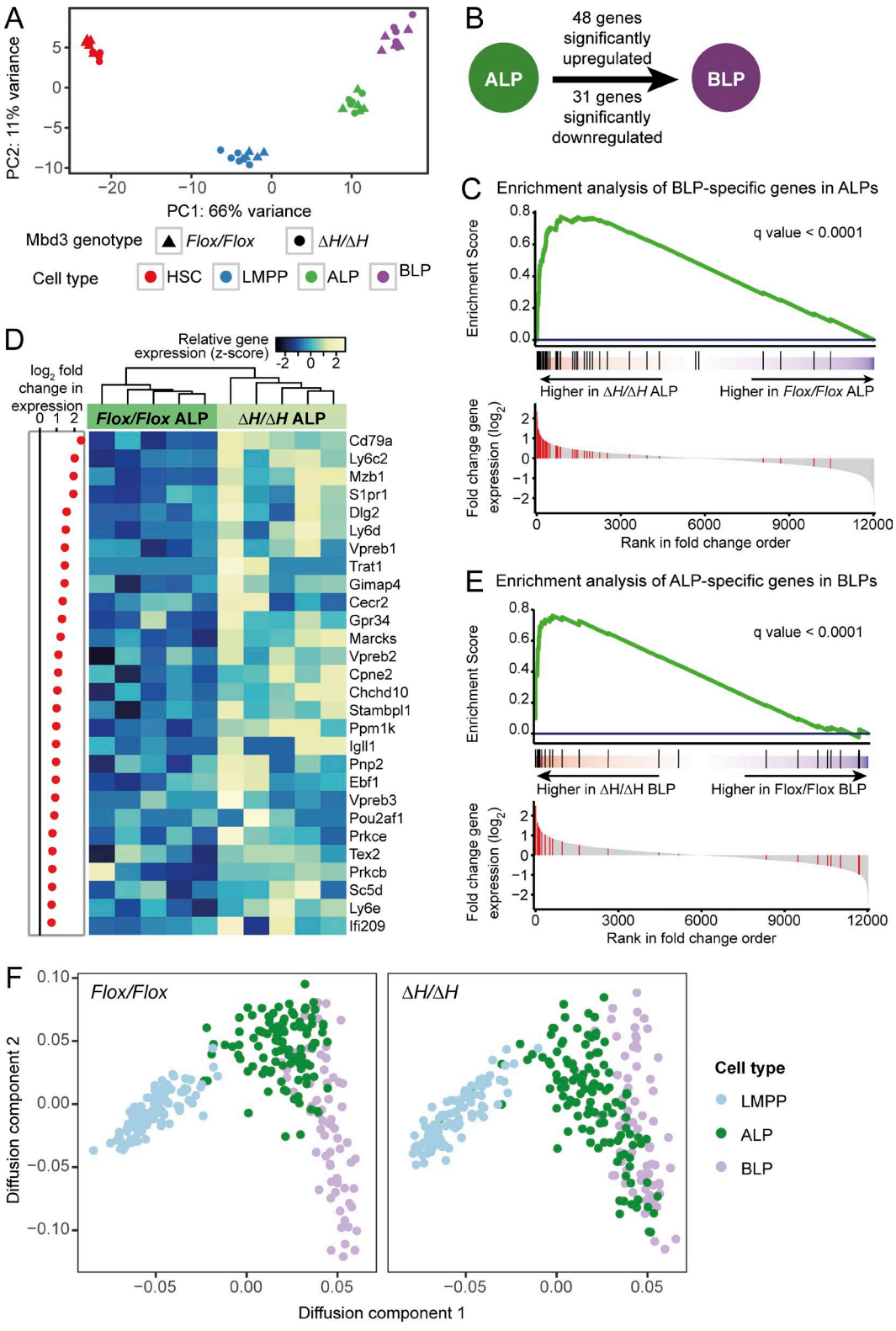

Figure 6. **Global transcriptome analysis reveals premature expression of B cell lineage commitment genes in Mbd3/NuRD-deficient lymphoid progenitors.** (A) Principal-component analysis of global gene expression in lymphoid progenitors ($n = 5$). (B) Schematic showing the number of significantly differentially expressed genes in *Mbd3*$^{Flox/Flox}$ BLPs compared with *Mbd3*$^{Flox/Flox}$ ALPs (false discovery rate < 0.05). (C) Gene set enrichment analysis (GSEA) enrichment score curve analyzing the distribution of the set of genes up-regulated during the transition from normal ALPs to BLPs in *Mbd3*$^{Flox/Flox}$ ALPs

mus, but those that do are able to respond appropriately to the thymic microenvironment and differentiate to maintain polyclonal T lymphopoiesis.

Compensatory hyperproliferation of ISP thymocytes and initiation of lymphoma

The effects of denying progenitor supply to the thymus have recently been studied using mouse models in which a normal thymus is transplanted into a recipient that cannot produce thymus-colonizing progenitors. In these studies, cells resident within the progenitor-deprived donor thymi, which would normally be replaced by freshly supplied progenitors, persist to sustain thymus-autonomous T cell development in the absence of ETPs (Martins et al., 2012, 2014; Peaudecerf et al., 2012). However, the changes to thymocyte cell biology that permit persistent, autonomous T cell production are poorly understood. Our data reveal that reduced supply of bone marrow progenitors to the thymus induces compensatory expansion and hyperproliferation of ISP thymocytes, and this is critical to maintaining normal thymocyte numbers. Previous analyses of progenitor-deprived thymi did not detect abnormal thymocyte proliferation but did not investigate the ISP population (Martins et al., 2012; Peaudecerf et al., 2012). In addition, persisting thymocytes in progenitor-deprived thymi give rise to T-ALL with an ISP-like phenotype, but the reason for this susceptibility to malignant transformation is not known (Martins et al., 2014). Rapid proliferation results in DNA replication stress and genomic instability (Gorgoulis et al., 2005; Gaillard et al., 2015), so our results suggest that compensatory hyperproliferation of ISPs in progenitor-deprived thymus may cause the accumulation of oncogenic mutations and transformation into T-ALL. Compensatory progenitor hyperproliferation could contribute to carcinogenesis in other tissues maintained by progenitor cells if early progenitor supply is disrupted.

Mbd3/NuRD chromatin remodeling inhibits activation of Ebf1 target genes

ALPs differentiate through a stage in which they express the B cell–specifying pioneer transcription factor Ebf1, but Ebf1-target genes are silent, and both B and T cell potential are retained (Mansson et al., 2010). Lack of cofactors, posttranslational regulation of the Ebf1 protein, and the expression of suppressor proteins have each been proposed to inhibit Ebf1-mediated transcription and prevent premature B cell commitment in these progenitors, but there is little evidence supporting these mechanisms (Mansson et al., 2010). Our data indicate that Mbd3/NuRD inhibits premature Ebf1 target gene activation in Ebf1-positive lymphoid progenitors and delays the commitment of bipotent B/T lymphoid progenitors to the B cell lineage. Although the timing of Ebf1 target gene activation is altered in Mbd3/NuRD-deficient cells, overall gene expression patterns during B cell differentiation are not broadly aberrant. This suggests that Mbd3/NuRD-mediated chromatin remodeling acts as a barrier that delays the transcriptional activation of Ebf1 targets but does not control which loci are targeted by Ebf1 binding. This is consistent with the ability of Ebf1 to bind its target loci even when they are embedded in naive, inaccessible chromatin (Boller et al., 2016).

Mbd3/NuRD controls B versus T lineage fate by inhibiting the accessibility of B cell–associated chromatin

Chromatin at pro–B cell enhancers and promoters is made more accessible during B cell specification, especially during the transition from BLP to pro–B cells (Bossen et al., 2015). Ebf1 binds its targets in inaccessible chromatin, and recruits the Brg1/BAF CRC, which depletes nucleosomes to initiate chromatin accessibility (Gao et al., 2009; Bossen et al., 2015; Boller et al., 2016). We found that regions that are opened during normal B cell differentiation are prematurely accessible in Mbd3-null ALPs. We also found that B cell enhancer and promoter regions are prematurely accessible in *Mbd3*-null BLPs and more accessible in *Mbd3*-null pro–B cells. These data indicate that Mbd3/NuRD chromatin remodeling opposes the ability of B cell programming factors to increase chromatin accessibility. The enhanced accessibility caused by Mbd3 deletion is more pronounced in BLPs and pro–B cells than ALPs. This is most likely because only a subset of ALPs in the population have so far undergone chromatin modeling to increase accessibility and because of the higher expression and activity of B cell programming factors that activate chromatin in the more differentiated cells (Inlay et al., 2009; Bossen et al., 2015).

The concept of Mbd3/NuRD and Brg1/BAF having antagonistic effects is consistent with knockdown studies in ES cells and also the observation that Brg1 and the Mbd3/NuRD component Chd4 have opposing effects on *Cd79a* chromatin accessibility and expression (Gao et al., 2009; Yildirim et al., 2011). We propose a model in which the balance of

compared with $Mbd3^{\Delta H/\Delta H}$ ALPs. Top: Kolmogorov-Smirnov running enrichment score. Bottom: location of the genes in this set in the list of gene expression changes between $Mbd3^{Flox/Flox}$ ALPs and $Mbd3^{\Delta H/\Delta H}$ ALPs, ranked by fold change. (D) Heat map showing the relative expression of the leading-edge gene subset from GSEA of BLP-specific genes in $Mbd3^{Flox/Flox}$ ALPs versus $Mbd3^{\Delta H/\Delta H}$ ALPs. Left: calculated fold change in expression ($\log_2$ transformed); right: relative gene expression detected in each sample (gene-normalized *z*-score). (E) GSEA enrichment score curve analyzing the distribution of the set of genes down-regulated during the transition from normal ALPs to BLPs in $Mbd3^{Flox/Flox}$ BLPs compared with $Mbd3^{\Delta H/\Delta H}$ BLPs. All data in A–E summarize five independent experiments sorting cells from sex-matched littermate mice. (F) Diffusion map dimensionality reduction analysis of gene expression in single cells measured by RNA-seq. The analysis includes the expression patterns of 289 genes that change significantly during the differentiation of $Mbd3^{Flox/Flox}$ LMPPs into BLPs. Mapping was performed on $Mbd3^{Flox/Flox}$ and $Mbd3^{\Delta H/\Delta H}$ cells together, but cells of each genotype are depicted in separate plots. Data summarize two independent experiments sorting cells from sex-matched littermate mice.

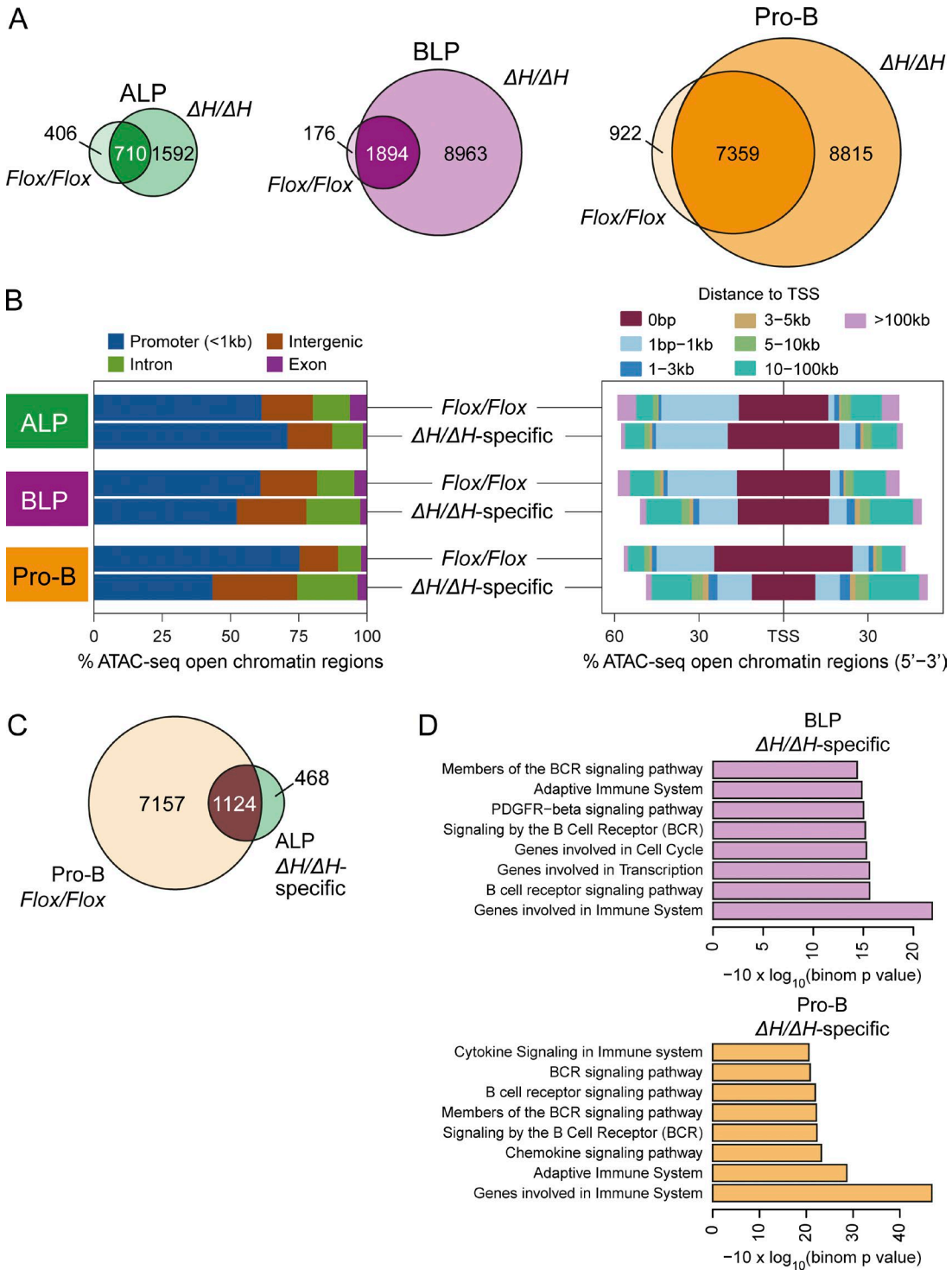

Figure 7. **Accessible chromatin regions in Mbd3/NuRD-deficient lymphoid progenitors.** (A) Number of accessible chromatin regions detected in lymphoid progenitor cells by ATAC-seq. The number of regions specific or common to *Mbd3*$^{Flox/Flox}$ and *Mbd3*$^{\Delta H/\Delta H}$ cells of each type is shown. (B) Genomic features associated with accessible chromatin regions. Left: the percentage of accessible chromatin regions associated with each genomic feature. Right: the distance and direction of accessible chromatin regions relative to the nearest transcriptional start site (TSS). The accessible regions detected in *Mbd3*$^{Flox/Flox}$ cells are shown, as well as those which are detected only in *Mbd3*$^{\Delta H/\Delta H}$ cells of the same type. (C) Number of accessible chromatin regions specific or common to *Mbd3*$^{\Delta H/\Delta H}$ ALPs and *Mbd3*$^{Flox/Flox}$ pro–B cells. (D) Most significant gene sets detected by Gene Ontology analysis of genes associated with accessible regions detected in *Mbd3*$^{\Delta H/\Delta H}$ BLPs and pro–B cells, but not in corresponding *Mbd3*$^{Flox/Flox}$ controls. All data are this figure summarizes two independent experiments in which cells were sorted from sex-matched littermate mice.

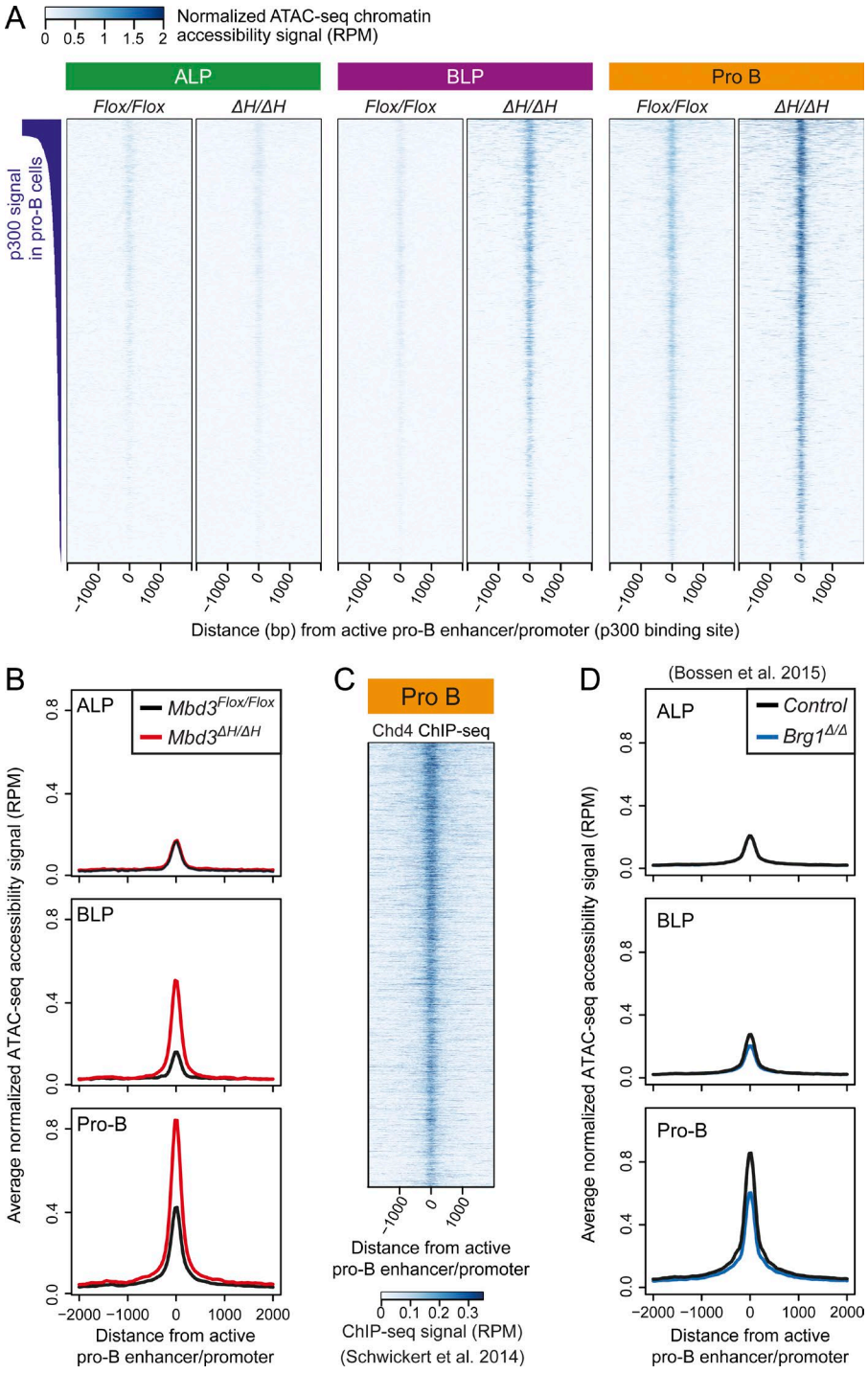

Figure 8. **Mbd3/NuRD–mediated chromatin remodeling restricts the accessibility of enhancers and promoters activated during B cell lineage specification.** (A) ATAC-seq chromatin accessibility signal in sorted *Mbd3*$^{Flox/Flox}$ and *Mbd3*$^{\Delta H/\Delta H}$ lymphoid progenitor cells, at 3,741 active enhancer and promoter regions associated with p300 binding in WT pro–B cells. Regions are ordered by the significance of the p300 signal in pro–B cells. Color intensity shows the number of ATAC-seq reads per million. (B) Mean ATAC-seq signal in sorted lymphoid progenitor cells, at all regions associated with p300 binding in WT pro–B cells (same regions shown in A). (C) Chd4 ChIP-seq signals in WT pro–B cells at the same regions shown in A. (D) Mean ATAC-seq signal in *Brg1*-deleted and control cells, at the same regions shown in A. All data in this figure summarize two independent experiments in which cells were sorted from sex-matched littermate mice.

Mbd3/NuRD and Brg1/BAF chromatin remodeling activities controls the fate of B/T-bipotent lymphoid progenitors by regulating the accessibility of enhancers and promoters associated with a B cell transcriptional program. In this model, a B cell–specifying pioneer transcription factor (e.g., Ebf1) recruits Brg1/BAF to latent B cell lineage-specific enhancers and promoters, which promotes chromatin accessibility at these regions (Gao et al., 2009; Bossen et al., 2015; Boller et al., 2016). The repressive chromatin remodeling activity of Mbd3/NuRD bound at these sites opposes the activity of Brg1/BAF, and thus inhibits their accessibility (Fig. 9). Mbd3/NuRD is therefore essential to prevent multipotent lymphoid progenitors prematurely activating expression of a B cell transcriptional program and committing to the B cell lineage. Expression of Brg1 increases significantly during B cell specification from the LMPP stage onwards (Bossen et al.,

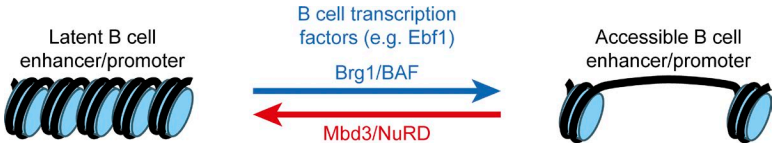

Figure 9. **Opposing activities of Mbd3/NuRD and Brg1/BAF control chromatin accessibility during B cell programming of multipotent lymphoid progenitors.** Commitment to the B cell lineage requires activation of dormant B cell–specific enhancers and promoters, embedded in inaccessible chromatin. Pioneering B cell transcription factors (e.g., Ebf1) bind to specific sequences in inaccessible chromatin and recruit Brg1/BAF, which remodels nucleosomes to make B cell–specific enhancers and promoters accessible. The repressive chromatin remodeling activity of Mbd3/NuRD limits the accessibility of these regions, preventing premature activation of a B cell transcriptional program.

2015). This likely explains why Mbd3/NuRD is specifically required during hematopoiesis to inhibit B cell differentiation in lymphoid progenitors.

Mbd3/NuRD can inhibit lineage commitment of progenitors by constraining the accessibility of dormant lineage-specific enhancers and promoters

Mbd3/NuRD promotes differentiation and lineage commitment of ES cells in response to appropriate signals, by inhibiting and silencing the established pluripotency-associated transcriptional program (Reynolds et al., 2012a,b; Whyte et al., 2012; Miller et al., 2016). Consistent with this mechanism, we found that Mbd3/NuRD was necessary for the complete silencing of ALP-specific genes during their differentiation into BLPs. However our results also reveal a novel mechanism by which Mbd3/NuRD chromatin remodeling can regulate the differentiation of multipotent cells: by constraining the activation of inaccessible chromatin to inhibit differentiation. This mechanism is crucially different, as it demonstrates that Mbd3/NuRD can act as a barrier to prevent lineage-specific transcription factors from prematurely enacting lineage commitment. Therefore, our data demonstrate that the regulation of multilineage differentiation by Mbd3/NuRD is complex, acting differently in different cellular contexts. This is most likely because the outcome of reduced chromatin accessibility mediated by Mbd3/NuRD is influenced by the current state of the chromatin landscape, and the activities of other CRCs and transcription factors in the cell. Because Mbd3/NuRD is ubiquitously expressed, it is likely that Mbd3/NuRD regulates many cell fate decisions during development by the novel mechanism we describe here: opposing the transcriptional pioneering of dormant enhancers induced by lineage-specific "master regulator" transcription factors.

MATERIALS AND METHODS

Mice

Vav-Cre (Stadtfeld and Graf, 2005) mice were backcrossed twice to C57BL/6 mice, then bred with mice from the floxed Mbd3 (Aguilera et al., 2011) mouse line, which had a 129/Ola genetic background. Mice were housed in specific pathogen-free conditions. PCR primers used to identify intact, floxed, and Cre-recombined Mbd3 alleles were 5′-TTG GTACAGACCAGGTGCAG-3′, 5′-AATCAGATCACT TCAGCTCC-3′, and 5′-CGAAACCATGATAAAGTC CC-3′. All procedures were performed according to UK Home Office regulations.

Nuclear protein extraction, coimmunoprecipitation, and immunoblots

Whole bone marrow, spleen, and thymus cells were washed once with PBS, then lysed in hypotonic lysis buffer (10 mM Hepes, pH 7.9, 10 mM KCl, 1.5 mM $MgCl_2$, 1 mM DTT, and cOmplete protease inhibitors; Roche). After 10 s of vortexing, nuclei were pelleted by centrifugation (10,000 *g*, 1 min), then resuspended in nuclear extraction buffer (10 mM Hepes, pH 7.9, 420 mM NaCl, 10 mM KCl, 1.5 mM $MgCl_2$, 0.1 mM EDTA, 12.5% [vol/vol] glycerol, 1 mM DTT, and cOmplete protease inhibitors). After 15 min incubation, and homogenization by repeatedly passing through a 23-gauge needle, insoluble material was pelleted by centrifugation (20,000 *g*, 5 min). The supernatant was retained as nuclear extract. For immunoblotting, each lane was loaded with 150 µg protein. For coimmunoprecipitation, 10 µg anti-Chd4 antibody was mixed with 50 µL of protein G Dynabeads (Thermo Fisher Scientific) and incubated overnight. After washing the beads three times in immunoprecipitation wash buffer (PBS with 0.02% [vol/vol] Tween-20), 150 µg nuclear extract protein was added. After 4 h, beads were then washed five times with immunoprecipitation wash buffer. Proteins were eluted from beads in SDS-PAGE loading buffer before immunoblot analysis. Antibodies used are shown in Table S2.

Flow cytometry

Cell suspensions were stained with antibodies shown in Table S2. Cell viability was determined by the exclusion of either 7AAD or DAPI. For Ki-67 analysis, cell surface antigens were stained first, then intracellular Ki-67 was stained using the BD Fixation/Permeabilization Solution kit (BD Biosciences). Cell sorting was performed using a FACSAria (BD Biosciences); cells with appropriate surface phenotypes were first sorted into separate tubes using "enrichment" precision mode. These cells were sorted again, and those still determined to have the appropriate cell surface phenotype were

sorted directly into lysis buffer or tissue culture medium using "single cell" or "purity" precision mode.

Thymocyte clonality analysis

PCR of D-J regions of the *Tcrb* locus was performed using previously described primers (Whitehurst et al., 1999); D1J1fwd: 5′-ACCTATGGGAGGGTCCTTTTT TGTATAAAG-3′; D1J2rev: 5′-AGACTCCTAGAC TGCAGACTCAG-3′; D2J2_fwd: 5′-AAAGCTGTA ACATTGTGGGGACAG-3′; and D2J2_rev: 5′-CCC GGAGATTCCCTAACCCTGGTC-3′.

Analysis of mutations in *Notch1*

Genomic DNA was isolated from T-ALL thymomas using a DNeasy Mini kit (QIAGEN). To identify point mutations, DNA from five T-ALLs was mixed together, then Notch1-coding exons were amplified using primers shown in Table S3. PCR products were then mixed together, blunt-ended, and ligated together. The ligated PCR products were sheared by sonication, and sequencing libraries were prepared. Sequencing was performed on an Illumina NextSeq, and reads were aligned to the mouse reference genome using STAR (Dobin et al., 2013). Potential mutations were identified at sites where >1% of the reads differed from the reference genome. The presence of mutations at these sites was then determined by Sanger sequencing of genomic DNA from each thymoma. Deletions in the Notch1 locus were detected as previously described (Ashworth et al., 2010), and deletions were sequenced by Sanger sequencing.

Quantitative RT-RCR (qRT-PCR)

For analysis of Notch1 target gene expression in thymocytes, RNA was isolated using an RNeasy Mini kit, and qRT-PCR was performed using a TaqMan RNA-to-Ct 1-Step kit (Thermo Fisher Scientific). The TaqMan assays used for the quantitation of each mRNA were *Hes1* Mm01342805_m1, *Dtx1* Mm00492297_m1, and *Myc* Mm00487804_m1. Gene expression was normalized to the expression of the housekeeping gene *Polr2a* (Mm00839493_m1).

In vitro lymphocyte differentiation cultures

To evaluate B cell lineage potential, cells were sorted onto a monolayer of OP9 stromal cells in OP9 medium (Opti-MEM medium with GlutaMAX [Thermo Fisher Scientific] with 10% FCS and 0.5 mM 2-mercaptoethanol) with 25 ng/ml mouse Flt3 ligand, 25 ng/ml mouse SCF, and 20 ng/ml mouse IL-7. Medium and cytokines were changed after 7 d, and B cell potential was evaluated by flow cytometry after 14 d of culture. Single cells that formed cultures containing at least 10 $B220^+$ $CD19^+$ cells were determined to have B cell potential. To analyze the rate of B cell differentiation, a portion of each culture was taken for flow cytometric analysis daily, and this volume was replaced by OP9 medium with cytokines. To evaluate T cell lineage potential, cells were sorted onto a monolayer of OP9-DL1 cells in OP9 medium with 50 ng/ml mouse Flt3 ligand, 25 ng/ml mouse SCF, and 20 ng/ml mouse IL-7. Medium and cytokines were changed weekly, and T cell potential was evaluated after 21 d of culture. Single cells that formed cultures containing at least 10 $Thy1.2^+$ $CD25^+$ and/or $CD4^+$ $CD8^+$ cells were determined to have T cell potential.

Single-cell qRT-PCR

Single-cell gene expression analysis was performed using 48.48 Dynamic Array integrated fluidics chips (M48; Fluidigm) on the BioMark HD platform (Fluidigm) as previously described (Moignard et al., 2013). TaqMan assays (Life Technologies) used are listed in Table S1. To measure expression of sterile IgH, a custom probe set was used, as previously described (Zandi et al., 2008). Raw C_T values are given in Table S4. Dimensionality reduction was applied to the single-cell qRT-PCR data with both genotypes analyzed together. First, amplification curves with a quality score <0.5 were treated as failed reactions. Gene expression was then normalized on a cellwise basis to the housekeeping gene *Polr2a*. A ΔCt value of −12 was assigned where a gene was not detected. Housekeeping genes *Ubc* and *Polr2a*, along with two genes not expressed in any cells (*Cd3e* and *Ptcra*), were excluded from further analysis. Diffusion map dimensionality reduction (Coifman et al., 2005; Haghverdi et al., 2015) was performed using the destiny R package (Angerer et al., 2016) with centered cosine distance and sigma = 0.5. Pseudotime values were assigned to single cells by applying the Wanderlust algorithm (Bendall et al., 2014) to coordinates of cells in diffusion components 1 and 2, which were selected on the basis of the magnitudes of their corresponding eigenvalues. To identify genes with expression related to differentiation of HSCs toward BLPs, cells were split into 100 bins of equal length in pseudotime. For each gene, the Spearman's rank correlation coefficient of the proportion of cells in a bin expressing the gene and the position of the bin in pseudotime was calculated using the cor.test function in R. Genes showing significant positive correlation with pseudotime values (Benjamini-Hochberg adjusted $P < 0.05$) were identified.

RNA-seq of populations of sorted cells

100 cells were FACS-sorted into 4 µl lysis buffer (0.2% [vol/vol\ Triton X-100 and 1 U/µl RNase inhibitor [Clontech]). RNA-seq libraries were prepared from five replicates of each cell type using the Smart-seq2 protocol (Picelli et al., 2013) and sequenced on an Illumina HiSeq 2500. Reads were aligned to the mouse genome using STAR (Dobin et al., 2013). The number of reads aligning to each gene were counted using HTSeq (Anders et al., 2015), and differential gene expression was analyzed using the R package DESeq2 (Love et al., 2014). Principal component analysis was performed using the *prcomp* function in R. Gene set enrichment analysis was performed using the R package DOSE (Yu et al., 2015).

Single-cell RNA-seq

Single-cell RNA-seq libraries were generated and sequenced from single sorted cells as previously described (Wilson et al., 2015). Sequencing reads were aligned to the mouse genome using G-SNAP (Wu and Nacu, 2010), and mapped reads were assigned to Ensembl genes (release 81; Yates et al., 2016) by using HTSeq (Anders et al., 2015). Cells with >15% of mapped reads mapping to mitochondrial genes, <200,000 reads mapping to nuclear genes, >40% of mapped reads mapping to ERCC spike-ins, or <1,000 genes with least 10 reads in the cell mapping to that gene were filtered out during quality control. 183 of 192 LMPP, 227 of 336, ALP and 140 of 144 BLP cells passed this quality control. Normalization size factors were computed using the scran R package (Lun et al., 2016), and 4,213 genes with variance exceeding technical levels were identified following the method of Brennecke et al. (2013). Differential gene expression analysis between populations of single cells was performed using the edgeR package (Robinson et al., 2010). Diffusion map dimensionality reduction was performed using the destiny R package (Haghverdi et al., 2015). Diffusion map embedding was calculated for both $Mbd3^{\Delta H/\Delta H}$ and control cells together, and the two conditions were then plotted separately.

ATAC-seq chromatin accessibility analysis

ATAC-seq libraries were prepared from 500 sorted cells as previously described (Buenrostro et al., 2013). Libraries underwent paired-end sequencing (2 × 125 nt) on an Illumina HiSeq 2500 instrument. After checking quality control with FastQC v.0.11.4, Nextera transposase sequence and adapter read-through were removed using Trimmomatic v.0.33 (Bolger et al., 2014) in palindrome mode with parameters LEADING:3 TRAILING:3 SLIDINGWINDOW:4:20 MIN LEN:35. Trimmed reads were aligned to the mouse reference genome using Bowtie2 v.2.2.3 (Langmead and Salzberg, 2012) with standard parameters except for –X 2,000 to allow for a maximum insert size of 2 kb. Alignment files were converted to Bam format with SAMtools v.1.2 (Li et al., 2009) and deduplicated using Picard MarkDuplicates v.1.119 (http://picard.sourceforge.net) with parameter REMOVE_DUPLICATES = true. Reads mapping to the mitochondrial genome were discarded, and alignment files were merged across replicates and indexed with BamTools v.2.4.0 (Barnett et al., 2011). ATAC-seq peaks were called using the findPeaks algorithm implemented in the Homer v.4.9 suite, with parameters –localSize 50,000 –size 150 –minDist 50 (Heinz et al., 2010). ATAC-seq data from Brg1-deficient mice (Bossen et al., 2015) were retrieved from the Short Read Archive (accession no. SRA246957), converted to fastq format using the SRA Toolkit v.2.5.4, and processed the same way we processed our own ATAC-seq data, with appropriate adjustments for single-end reads. Genomic coordinates of p300 binding sites in pro–B cells (Lin et al., 2012) were downloaded from the Gene Expression Omnibus (accession no. GSM987808) and lifted over to mm10 using the UCSC liftOver utility. Chd4 ChIP-seq data in $Ikzf1^{\Delta/+}$ pro–B cells (Schwickert et al., 2014) were downloaded from NCBI SRA (accession nos. SRX398246 and SRX398233), converted to fastq format, and aligned using Bowtie2. Downstream computational analyses were performed using R v.3.2.2 (R Core Team, 2015) and BioConductor v.3.2 (Huber et al., 2015). Heat maps and metaprofiles of ATAC-seq signals were computed using custom scripts and the Genomation package v.1.3.4 (Akalin et al., 2015).

Data availability

Raw and processed data from bulk cell population RNA-seq, single-cell RNA-seq, and ATAC-seq experiments have been deposited in the Gene Expression Omnibus (accession no. GSE101735). Raw single-cell qPCR data are available in Table S4.

Online supplemental material

Fig. S1 shows cell counts from mouse peripheral blood, thymus, and bone marrow. Fig. S2 shows the *Notch1* mutations, and activation of Notch1 target genes, detected in $Mbd3^{\Delta H/\Delta H}$ T-ALLs. Fig. S3 shows that a subset of cells in Hardy fractions B and C from $Mbd3^{\Delta H/\Delta H}$ bone marrow express abnormally high levels of c-Kit. Fig. S4 shows pseudotime ordering of single-cell gene expression patterns, the proportion of single ALP cells that express genes associated with B cell differentiation, and the level of *Ebf1* expression in single ALPs. Fig. S5 shows ATAC-seq data that indicate that normal chromatin accessibility is normal in $Mbd3^{\Delta H/\Delta H}$ thymocytes. Table S1 shows the assays used to measure single-cell gene expression. Table S2 lists the antibodies used in the study. Table S3 lists the oligos used for identifying point mutations in Notch1. Tables S4–S11 are available as Excel spreadsheets. Table S4 provides the raw data from the single-cell qRT-PCR experiment. Differential gene expression analysis is provided comparing $Mbd3^{\Delta H/\Delta H}$ cells to control cells from the HSC (Table S5), LMPP (Table S6), ALP (Table S7), and BLP (Table S8) populations. Table S9 provides the list of genes different between control LMPPs and BLPs, used for the dimensionality reduction analysis in Fig. 6 F. Table S10 provides differential gene expression analysis of single-cell RNA-seq data, comparing $Mbd3^{\Delta H/\Delta H}$ ALPs to control ALPs. Table S11 lists the regions of accessible chromatin detected in $Mbd3^{\Delta H/\Delta H}$ and control ALPs, BLPs, and pro–B cells.

ACKNOWLEDGMENTS

We thank Tina Hamilton and Dean Pask for assistance with animal husbandry, Hesham Eldaly for assistance with histopathology, and David Flores-Santa-Cruz for assistance with bioinformatic analysis.

F. Comoglio was supported by a European Molecular Biology Organization long-term fellowship (1305-2015 and Marie Curie Actions LTFCOFUND2013/GA-2013-609409). Work in the Green laboratory is supported by Cancer Research UK (grants C1163/A12765 and C1163/A12526), Bloodwise (grant 13003), and core support grants by the Wellcome Trust to the Cambridge Institute for Medical Research (grant 100140/Z/12/Z) and Wellcome Trust–MRC Cambridge Stem Cell Institute (grant 097922/Z/11/Z).

The authors declare no competing financial interests.

Author contributions: S. J. Loughran designed and performed experiments, analyzed data, and wrote the paper. F. Comoglio and F.K. Hamey analyzed data. A. Giustacchini, Y. Errami, and E. Earp performed experiments. B. Göttgens, S.E.W. Jacobsen, and A.J. Mead contributed analytic tools, as well as advice and input on experimental design. B. Hendrich provided reagents and designed experiments. A.R. Green supervised the study and wrote the paper.

Submitted: 30 October 2016

Revised: 4 July 2017

Accepted: 25 July 2017

REFERENCES

Adolfsson, J., R. Månsson, N. Buza-Vidas, A. Hultquist, K. Liuba, C.T. Jensen, D. Bryder, L. Yang, O.-J. Borge, L.A.M. Thoren, et al. 2005. Identification of Flt3+ lympho-myeloid stem cells lacking erythro-megakaryocytic potential: A revised road map for adult blood lineage commitment. *Cell*. 121:295–306. http://dx.doi.org/10.1016/j.cell.2005.02.013

Aguilera, C., K. Nakagawa, R. Sancho, A. Chakraborty, B. Hendrich, and A. Behrens. 2011. c-Jun N-terminal phosphorylation antagonises recruitment of the Mbd3/NuRD repressor complex. *Nature.* 469:231–235. http://dx.doi.org/10.1038/nature09607

Ahringer, J. 2000. NuRD and SIN3: histone deacetylase complexes in development. *Trends Genet*. 16:351–356. http://dx.doi.org/10.1016/S0168-9525(00)02066-7

Akalin, A., V. Franke, K. Vlahoviček, C.E. Mason, and D. Schübeler. 2015. Genomation: A toolkit to summarize, annotate and visualize genomic intervals. *Bioinformatics.* 31:1127–1129. http://dx.doi.org/10.1093/bioinformatics/btu775

Anders, S., P.T. Pyl, and W. Huber. 2015. HTSeq—A Python framework to work with high-throughput sequencing data. *Bioinformatics.* 31:166–169. http://dx.doi.org/10.1093/bioinformatics/btu638

Angerer, P., L. Haghverdi, M. Büttner, F.J. Theis, C. Marr, and F. Buettner. 2016. destiny: diffusion maps for large-scale single-cell data in R. *Bioinformatics.* 32:1241–1243. http://dx.doi.org/10.1093/bioinformatics/btv715

Ashworth, T.D., W.S. Pear, M.Y. Chiang, S.C. Blacklow, J. Mastio, L. Xu, M. Kelliher, P. Kastner, S. Chan, and J.C. Aster. 2010. Deletion-based mechanisms of Notch1 activation in T-ALL: Key roles for RAG recombinase and a conserved internal translational start site in Notch1. *Blood*. 116:5455–5464. http://dx.doi.org/10.1182/blood-2010-05-286328

Aster, J.C., S.C. Blacklow, and W.S. Pear. 2011. Notch signalling in T-cell lymphoblastic leukaemia/lymphoma and other haematological malignancies. *J. Pathol.* 223:263–273. http://dx.doi.org/10.1002/path.2789

Barnett, D.W., E.K. Garrison, A.R. Quinlan, M.P. Strömberg, and G.T. Marth. 2011. BamTools: A C++ API and toolkit for analyzing and managing BAM files. *Bioinformatics.* 27:1691–1692. http://dx.doi.org/10.1093/bioinformatics/btr174

Bendall, S.C., K.L. Davis, A.D. Amir, M.D. Tadmor, E.F. Simonds, T.J. Chen, D.K. Shenfeld, G.P. Nolan, and D. Pe'er. 2014. Single-cell trajectory detection uncovers progression and regulatory coordination in human B cell development. *Cell*. 157:714–725. http://dx.doi.org/10.1016/j.cell.2014.04.005

Bolger, A.M., M. Lohse, and B. Usadel. 2014. Trimmomatic: A flexible trimmer for Illumina sequence data. *Bioinformatics.* 30:2114–2120. http://dx.doi.org/10.1093/bioinformatics/btu170

Boller, S., S. Ramamoorthy, D. Akbas, R. Nechanitzky, L. Burger, R. Murr, D. Schübeler, and R. Grosschedl. 2016. Pioneering activity of the C-terminal domain of EBF1 shapes the chromatin landscape for B cell programming. *Immunity.* 44:527–541. http://dx.doi.org/10.1016/j.immuni.2016.02.021

Bossen, C., C.S. Murre, A.N. Chang, R. Mansson, H.R. Rodewald, and C. Murre. 2015. The chromatin remodeler Brg1 activates enhancer repertoires to establish B cell identity and modulate cell growth. *Nat. Immunol.* 16:775–784. http://dx.doi.org/10.1038/ni.3170

Brennecke, P., S. Anders, J.K. Kim, A.A. Kołodziejczyk, X. Zhang, V. Proserpio, B. Baying, V. Benes, S.A. Teichmann, J.C. Marioni, and M.G. Heisler. 2013. Accounting for technical noise in single-cell RNA-seq experiments. *Nat. Methods.* 10:1093–1095. http://dx.doi.org/10.1038/nmeth.2645

Buenrostro, J.D., P.G. Giresi, L.C. Zaba, H.Y. Chang, and W.J. Greenleaf. 2013. Transposition of native chromatin for fast and sensitive epigenomic profiling of open chromatin, DNA-binding proteins and nucleosome position. *Nat. Methods.* 10:1213–1218. http://dx.doi.org/10.1038/nmeth.2688

Ceredig, R., N. Bosco, and A.G. Rolink. 2007. The B lineage potential of thymus settling progenitors is critically dependent on mouse age. *Eur. J. Immunol.* 37:830–837. http://dx.doi.org/10.1002/eji.200636728

Chen, T., and S.Y.R. Dent. 2014. Chromatin modifiers and remodellers: Regulators of cellular differentiation. *Nat. Rev. Genet.* 15:93–106. http://dx.doi.org/10.1038/nrg3607

Coifman, R.R., S. Lafon, A.B. Lee, M. Maggioni, B. Nadler, F. Warner, and S.W. Zucker. 2005. Geometric diffusions as a tool for harmonic analysis and structure definition of data: diffusion maps. *Proc. Natl. Acad. Sci. USA*. 102:7426–7431. http://dx.doi.org/10.1073/pnas.0500334102

Decker, T., M. Pasca di Magliano, S. McManus, Q. Sun, C. Bonifer, H. Tagoh, and M. Busslinger. 2009. Stepwise activation of enhancer and promoter regions of the B cell commitment gene Pax5 in early lymphopoiesis. *Immunity.* 30:508–520. http://dx.doi.org/10.1016/j.immuni.2009.01.012

Dobin, A., C.A. Davis, F. Schlesinger, J. Drenkow, C. Zaleski, S. Jha, P. Batut, M. Chaisson, and T.R. Gingeras. 2013. STAR: Ultrafast universal RNA-seq aligner. *Bioinformatics.* 29:15–21. http://dx.doi.org/10.1093/bioinformatics/bts635

Dovey, O.M., C.T. Foster, N. Conte, S.A. Edwards, J.M. Edwards, R. Singh, G. Vassiliou, A. Bradley, and S.M. Cowley. 2013. Histone deacetylase 1 and 2 are essential for normal T-cell development and genomic stability in mice. *Blood*. 121:1335–1344. http://dx.doi.org/10.1182/blood-2012-07-441949

Fujita, N., D.L. Jaye, C. Geigerman, A. Akyildiz, M.R. Mooney, J.M. Boss, and P.A. Wade. 2004. MTA3 and the Mi-2/NuRD complex regulate cell fate during B lymphocyte differentiation. *Cell*. 119:75–86. http://dx.doi.org/10.1016/j.cell.2004.09.014

Gaillard, H., T. García-Muse, and A. Aguilera. 2015. Replication stress and cancer. *Nat. Rev. Cancer.* 15:276–289. http://dx.doi.org/10.1038/nrc3916

Gao, H., K. Lukin, J. Ramírez, S. Fields, D. Lopez, and J. Hagman. 2009. Opposing effects of SWI/SNF and Mi-2/NuRD chromatin remodeling complexes on epigenetic reprogramming by EBF and Pax5. *Proc. Natl. Acad. Sci. USA*. 106:11258–11263. http://dx.doi.org/10.1073/pnas.0809485106

Gorgoulis, V.G., L.-V.F. Vassiliou, P. Karakaidos, P. Zacharatos, A. Kotsinas, T. Liloglou, M. Venere, R.A. Ditullio Jr., N.G. Kastrinakis, B. Levy, et al. 2005. Activation of the DNA damage checkpoint and genomic instability in human precancerous lesions. *Nature.* 434:907–913. http://dx.doi.org/10.1038/nature03485

Haghverdi, L., F. Buettner, and F.J. Theis. 2015. Diffusion maps for high-dimensional single-cell analysis of differentiation data. *Bioinformatics.* 31:2989–2998. http://dx.doi.org/10.1093/bioinformatics/btv325

Heideman, M.R., R.H. Wilting, E. Yanover, A. Velds, J. de Jong, R.M. Kerkhoven, H. Jacobs, L.F. Wessels, and J.-H. Dannenberg. 2013. Dosage-dependent tumor suppression by histone deacetylases 1 and 2 through regulation of c-Myc collaborating genes and p53 function. *Blood*. 121:2038–2050. http://dx.doi.org/10.1182/blood-2012-08-450916

Heinz, S., C. Benner, N. Spann, E. Bertolino, Y.C. Lin, P. Laslo, J.X. Cheng, C. Murre, H. Singh, and C.K. Glass. 2010. Simple combinations of

lineage-determining transcription factors prime cis-regulatory elements required for macrophage and B cell identities. *Mol. Cell.* 38:576–589. http://dx.doi.org/10.1016/j.molcel.2010.05.004

Ho, L., and G.R. Crabtree. 2010. Chromatin remodelling during development. *Nature.* 463:474–484. http://dx.doi.org/10.1038/nature08911

Huber, W., V.J. Carey, R. Gentleman, S. Anders, M. Carlson, B.S. Carvalho, H.C. Bravo, S. Davis, L. Gatto, T. Girke, et al. 2015. Orchestrating high-throughput genomic analysis with Bioconductor. *Nat. Methods.* 12:115–121. http://dx.doi.org/10.1038/nmeth.3252

Inlay, M.A., D. Bhattacharya, D. Sahoo, T. Serwold, J. Seita, H. Karsunky, S.K. Plevritis, D.L. Dill, and I.L. Weissman. 2009. Ly6d marks the earliest stage of B-cell specification and identifies the branchpoint between B-cell and T-cell development. *Genes Dev.* 23:2376–2381. http://dx.doi.org/10.1101/gad.1836009

Kaji, K., I.M. Caballero, R. MacLeod, J. Nichols, V.A. Wilson, and B. Hendrich. 2006. The NuRD component Mbd3 is required for pluripotency of embryonic stem cells. *Nat. Cell Biol.* 8:285–292. http://dx.doi.org/10.1038/ncb1372

Kaji, K., J. Nichols, and B. Hendrich. 2007. Mbd3, a component of the NuRD co-repressor complex, is required for development of pluripotent cells. *Development.* 134:1123–1132. http://dx.doi.org/10.1242/dev.02802

Langmead, B., and S.L. Salzberg. 2012. Fast gapped-read alignment with Bowtie 2. *Nat. Methods.* 9:357–359. http://dx.doi.org/10.1038/nmeth.1923

Lara-Astiaso, D., A. Weiner, E. Lorenzo-Vivas, I. Zaretsky, D. Jaitin, E. David, H. Keren-Shaul, A. Mildner, D. Winter, S. Jung, et al. 2014. Chromatin state dynamics during blood formation. *Science.* 345:943–949. http://dx.doi.org/10.1126/science.1256271

Li, H., B. Handsaker, A. Wysoker, T. Fennell, J. Ruan, N. Homer, G. Marth, G. Abecasis, R. Durbin, G.P. Data, and T. Sam. 1000 Genome Project Data Processing Subgroup. 2009. The Sequence Alignment/Map format and SAMtools. *Bioinformatics.* 25:2078–2079. http://dx.doi.org/10.1093/bioinformatics/btp352

Lin, Y.C., C. Benner, R. Mansson, S. Heinz, K. Miyazaki, M. Miyazaki, V. Chandra, C. Bossen, C.K. Glass, and C. Murre. 2012. Global changes in the nuclear positioning of genes and intra- and interdomain genomic interactions that orchestrate B cell fate. *Nat. Immunol.* 13:1196–1204. http://dx.doi.org/10.1038/ni.2432

Love, M.I., W. Huber, and S. Anders. 2014. Moderated estimation of fold change and dispersion for RNA-seq data with DESeq2. *Genome Biol.* 15:550. http://dx.doi.org/10.1186/s13059-014-0550-8

Luc, S., T.C. Luis, H. Boukarabila, I.C. Macaulay, N. Buza-Vidas, T. Bouriez-Jones, M. Lutteropp, P.S. Woll, S.J. Loughran, A.J. Mead, et al. 2012. The earliest thymic T cell progenitors sustain B cell and myeloid lineage potential. *Nat. Immunol.* 13:412–419. http://dx.doi.org/10.1038/ni.2255

Lun, A.T.L., K. Bach, and J.C. Marioni. 2016. Pooling across cells to normalize single-cell RNA sequencing data with many zero counts. *Genome Biol.* 17:75. http://dx.doi.org/10.1186/s13059-016-0947-7

Maier, H., R. Ostraat, H. Gao, S. Fields, S.A. Shinton, K.L. Medina, T. Ikawa, C. Murre, H. Singh, R.R. Hardy, and J. Hagman. 2004. Early B cell factor cooperates with Runx1 and mediates epigenetic changes associated with mb-1 transcription. *Nat. Immunol.* 5:1069–1077. http://dx.doi.org/10.1038/ni1119

Mansson, R., S. Zandi, E. Welinder, P. Tsapogas, N. Sakaguchi, D. Bryder, and M. Sigvardsson. 2010. Single-cell analysis of the common lymphoid progenitor compartment reveals functional and molecular heterogeneity. *Blood.* 115:2601–2609. http://dx.doi.org/10.1182/blood-2009-08-236398

Mansson, R., E. Welinder, J. Åhsberg, Y.C. Lin, C. Benner, C.K. Glass, J.S. Lucas, M. Sigvardsson, and C. Murre. 2012. Positive intergenic feedback circuitry, involving EBF1 and FOXO1, orchestrates B-cell fate. *Proc. Natl. Acad. Sci. USA.* 109:21028–21033. http://dx.doi.org/10.1073/pnas.1211427109

Martins, V.C., E. Ruggiero, S.M. Schlenner, V. Madan, M. Schmidt, P.J. Fink, C. von Kalle, and H.-R. Rodewald. 2012. Thymus-autonomous T cell development in the absence of progenitor import. *J. Exp. Med.* 209:1409–1417. http://dx.doi.org/10.1084/jem.20120846

Martins, V.C., K. Busch, D. Juraeva, C. Blum, C. Ludwig, V. Rasche, F. Lasitschka, S.E. Mastitsky, B. Brors, T. Hielscher, et al. 2014. Cell competition is a tumour suppressor mechanism in the thymus. *Nature.* 509:465–470. http://dx.doi.org/10.1038/nature13317

McDonel, P., I. Costello, and B. Hendrich. 2009. Keeping things quiet: roles of NuRD and Sin3 co-repressor complexes during mammalian development. *Int. J. Biochem. Cell Biol.* 41:108–116. http://dx.doi.org/10.1016/j.biocel.2008.07.022

Menafra, R., and H.G. Stunnenberg. 2014. MBD2 and MBD3: Elusive functions and mechanisms. *Front. Genet.* 5:428. http://dx.doi.org/10.3389/fgene.2014.00428

Mercer, E.M., Y.C. Lin, C. Benner, S. Jhunjhunwala, J. Dutkowski, M. Flores, M. Sigvardsson, T. Ideker, C.K. Glass, and C. Murre. 2011. Multilineage priming of enhancer repertoires precedes commitment to the B and myeloid cell lineages in hematopoietic progenitors. *Immunity.* 35:413–425. http://dx.doi.org/10.1016/j.immuni.2011.06.013

Miller, A., M. Ralser, S.L. Kloet, R. Loos, R. Nishinakamura, P. Bertone, M. Vermeulen, and B. Hendrich. 2016. Sall4 controls differentiation of pluripotent cells independently of the nucleosome remodelling and deacetylation (NuRD) complex. *Development.* 143:3074–3084. http://dx.doi.org/10.1242/dev.139113

Moignard, V., I.C. Macaulay, G. Swiers, F. Buettner, J. Schütte, F.J. Calero-Nieto, S. Kinston, A. Joshi, R. Hannah, F.J. Theis, et al. 2013. Characterization of transcriptional networks in blood stem and progenitor cells using high-throughput single-cell gene expression analysis. *Nat. Cell Biol.* 15:363–372. http://dx.doi.org/10.1038/ncb2709

Naito, T., P. Gómez-Del Arco, C.J. Williams, and K. Georgopoulos. 2007. Antagonistic interactions between Ikaros and the chromatin remodeler Mi-2β determine silencer activity and Cd4 gene expression. *Immunity.* 27:723–734. http://dx.doi.org/10.1016/j.immuni.2007.09.008

Nutt, S.L., P. Urbánek, A. Rolink, and M. Busslinger. 1997. Essential functions of Pax5 (BSAP) in pro-B cell development: Difference between fetal and adult B lymphopoiesis and reduced V-to-DJ recombination at the IgH locus. *Genes Dev.* 11:476–491. http://dx.doi.org/10.1101/gad.11.4.476

Peaudecerf, L., S. Lemos, A. Galgano, G. Krenn, F. Vasseur, J.P. Di Santo, S. Ezine, and B. Rocha. 2012. Thymocytes may persist and differentiate without any input from bone marrow progenitors. *J. Exp. Med.* 209:1401–1408. http://dx.doi.org/10.1084/jem.20120845

Picelli, S., Å.K. Björklund, O.R. Faridani, S. Sagasser, G. Winberg, and R. Sandberg. 2013. Smart-seq2 for sensitive full-length transcriptome profiling in single cells. *Nat. Methods.* 10:1096–1098. http://dx.doi.org/10.1038/nmeth.2639

Reynolds, N., P. Latos, A. Hynes-Allen, R. Loos, D. Leaford, A. O'Shaughnessy, O. Mosaku, J. Signolet, P. Brennecke, T. Kalkan, et al. 2012a. NuRD suppresses pluripotency gene expression to promote transcriptional heterogeneity and lineage commitment. *Cell Stem Cell.* 10:583–594. http://dx.doi.org/10.1016/j.stem.2012.02.020

Reynolds, N., M. Salmon-Divon, H. Dvinge, A. Hynes-Allen, G. Balasooriya, D. Leaford, A. Behrens, P. Bertone, and B. Hendrich. 2012b. NuRD-mediated deacetylation of H3K27 facilitates recruitment of Polycomb Repressive Complex 2 to direct gene repression. *EMBO J.* 31:593–605. http://dx.doi.org/10.1038/emboj.2011.431

Reynolds, N., A. O'Shaughnessy, and B. Hendrich. 2013. Transcriptional repressors: Multifaceted regulators of gene expression. *Development.* 140:505–512. http://dx.doi.org/10.1242/dev.083105

Robinson, M.D., D.J. McCarthy, and G.K. Smyth. 2010. edgeR: A Bioconductor package for differential expression analysis of digital gene expression data. *Bioinformatics.* 26:139–140. http://dx.doi.org/10.1093/bioinformatics/btp616

Rossi, F.M.V., S.Y. Corbel, J.S. Merzaban, D.A. Carlow, K. Gossens, J. Duenas, L. So, L. Yi, and H.J. Ziltener. 2005. Recruitment of adult thymic progenitors is regulated by P-selectin and its ligand PSGL-1. *Nat. Immunol.* 6:626–634. http://dx.doi.org/10.1038/ni1203

Rumfelt, L.L., Y. Zhou, B.M. Rowley, S.A. Shinton, and R.R. Hardy. 2006. Lineage specification and plasticity in CD19- early B cell precursors. *J. Exp. Med.* 203:675–687. http://dx.doi.org/10.1084/jem.20052444

Schlenner, S.M., V. Madan, K. Busch, A. Tietz, C. Läufle, C. Costa, C. Blum, H.J. Fehling, and H.R. Rodewald. 2010. Fate mapping reveals separate origins of T cells and myeloid lineages in the thymus. *Immunity.* 32:426–436. http://dx.doi.org/10.1016/j.immuni.2010.03.005

Schwickert, T.A., H. Tagoh, S. Gültekin, A. Dakic, E. Axelsson, M. Minnich, A. Ebert, B. Werner, M. Roth, L. Cimmino, et al. 2014. Stage-specific control of early B cell development by the transcription factor Ikaros. *Nat. Immunol.* 15:283–293. http://dx.doi.org/10.1038/ni.2828

Serwold, T., L.I.R. Ehrlich, and I.L. Weissman. 2009. Reductive isolation from bone marrow and blood implicates common lymphoid progenitors as the major source of thymopoiesis. *Blood.* 113:807–815. http://dx.doi.org/10.1182/blood-2008-08-173682

Stadtfeld, M., and T. Graf. 2005. Assessing the role of hematopoietic plasticity for endothelial and hepatocyte development by non-invasive lineage tracing. *Development.* 132:203–213. http://dx.doi.org/10.1242/dev.01558

Ungerbäck, J., J. Åhsberg, T. Strid, R. Somasundaram, and M. Sigvardsson. 2015. Combined heterozygous loss of Ebf1 and Pax5 allows for T-lineage conversion of B cell progenitors. *J. Exp. Med.* 212:1109–1123. http://dx.doi.org/10.1084/jem.20132100

Visel, A., M.J. Blow, Z. Li, T. Zhang, J.A. Akiyama, A. Holt, I. Plajzer-Frick, M. Shoukry, C. Wright, F. Chen, et al. 2009. ChIP-seq accurately predicts tissue-specific activity of enhancers. *Nature.* 457:854–858. http://dx.doi.org/10.1038/nature07730

Whitehurst, C.E., S. Chattopadhyay, and J. Chen. 1999. Control of V(D)J recombinational accessibility of the D β 1 gene segment at the TCR β locus by a germline promoter. *Immunity.* 10:313–322. http://dx.doi.org/10.1016/S1074-7613(00)80031-X

Whyte, W.A., S. Bilodeau, D.A. Orlando, H.A. Hoke, G.M. Frampton, C.T. Foster, S.M. Cowley, and R.A. Young. 2012. Enhancer decommissioning by LSD1 during embryonic stem cell differentiation. *Nature.* 482:221–225.

Williams, C.J., T. Naito, P.G.-D. Arco, J.R. Seavitt, S.M. Cashman, B. De Souza, X. Qi, P. Keables, U.H. Von Andrian, and K. Georgopoulos. 2004. The chromatin remodeler Mi-2β is required for CD4 expression and T cell development. *Immunity.* 20:719–733. http://dx.doi.org/10.1016/j.immuni.2004.05.005

Wilson, N.K., D.G. Kent, F. Buettner, M. Shehata, I.C. Macaulay, F.J. Calero-Nieto, M. Sánchez Castillo, C.A. Oedekoven, E. Diamanti, R. Schulte, et al. 2015. Combined single-cell functional and gene expression analysis resolves heterogeneity within stem cell populations. *Cell Stem Cell.* 16:712–724. http://dx.doi.org/10.1016/j.stem.2015.04.004

Wu, T.D., and S. Nacu. 2010. Fast and SNP-tolerant detection of complex variants and splicing in short reads. *Bioinformatics.* 26:873–881. http://dx.doi.org/10.1093/bioinformatics/btq057

Yang, X.-J., and E. Seto. 2008. The Rpd3/Hda1 family of lysine deacetylases: From bacteria and yeast to mice and men. *Nat. Rev. Mol. Cell Biol.* 9:206–218. http://dx.doi.org/10.1038/nrm2346

Yates, A., W. Akanni, M.R. Amode, D. Barrell, K. Billis, D. Carvalho-Silva, C. Cummins, P. Clapham, S. Fitzgerald, L. Gil, et al. 2016. Ensembl 2016. *Nucleic Acids Res.* 44(D1):D710–D716. http://dx.doi.org/10.1093/nar/gkv1157

Yildirim, O., R. Li, J.-H. Hung, P.B.B. Chen, X. Dong, L.-S. Ee, Z. Weng, O.J.J. Rando, and T.G.G. Fazzio. 2011. Mbd3/NURD complex regulates expression of 5-hydroxymethylcytosine marked genes in embryonic stem cells. *Cell.* 147:1498–1510. http://dx.doi.org/10.1016/j.cell.2011.11.054

Yoshida, T., I. Hazan, J. Zhang, S.Y. Ng, T. Naito, H.J. Snippert, E.J. Heller, X. Qi, L.N. Lawton, C.J. Williams, and K. Georgopoulos. 2008. The role of the chromatin remodeler Mi-2β in hematopoietic stem cell self-renewal and multilineage differentiation. *Genes Dev.* 22:1174–1189. http://dx.doi.org/10.1101/gad.1642808

Yu, G., L. Wang, G. Yan, and Q. He. 2015. DOSE: An R/Bioconductor package for disease ontology semantic and enrichment analysis. *Bioinformatics.* 31:608–609. http://dx.doi.org/10.1093/bioinformatics/btu684

Yui, M.A., and E.V. Rothenberg. 2014. Developmental gene networks: A triathlon on the course to T cell identity. *Nat. Rev. Immunol.* 14:529–545. http://dx.doi.org/10.1038/nri3702

Zandi, S., R. Mansson, P. Tsapogas, J. Zetterblad, D. Bryder, and M. Sigvardsson. 2008. EBF1 is essential for B-lineage priming and establishment of a transcription factor network in common lymphoid progenitors. *J. Immunol.* 181:3364–3372. http://dx.doi.org/10.4049/jimmunol.181.5.3364

Zlotoff, D.A., A. Sambandam, T.D. Logan, J.J. Bell, B.A. Schwarz, and A. Bhandoola. 2010. CCR7 and CCR9 together recruit hematopoietic progenitors to the adult thymus. *Blood.* 115:1897–1905. http://dx.doi.org/10.1182/blood-2009-08-237784